High Temperature Processing Symposium 2010

8-9 February 2010
Engineering Building, EN715, EN515
Swinburne University of Technology

Final Program and Abstract Book

AUSMELT
GLOBAL ENVIROMETAL TECHNOLOGIES

CAST
CAST Cooperative Research Centre

FURNACE

SWINBURNE UNIVERSITY OF TECHNOLOGY

HIGH TEMPERATURE PROCESSING SYMPOSIUM 2010
Swinburne University of Technology
8 – 9 February 2010, Melbourne, Australia

Editors

Prof. Geoffrey Brooks

Dr M. Akbar Rhamdhani

Dr Xiadong Xu

Organising Committee

Prof. Geoffrey Brooks – GBrooks@swin.edu.au

Dr M. Akbar Rhamdhani – ARhamdhani@swin.edu.au

Dr Xiaodong Xu – XXu@swin.edu.au

Mr Brian Lightfoot – Blightfoot@swin.edu.au

Mr Morshed Alam – MMalam@swin.edu.au

Mr Pa Hmun – PaHmun@swin.edu.au

Mr Nazmul Huda – MHuda@swin.edu.au

Mr Madhu Kodappully – MKodappully@swin.edu.au

Published in Australia by: Faculty of Engineering and Industrial Sciences, Swinburne University of Technology

ISBN 978-0-9806708-0-6

HIGH TEMPERATURE PROCESSING SYMPOSIUM 2010
Swinburne University of Technology
8 – 9 February 2010, Melbourne, Australia

We wish to thank the main sponsors for their contribution to the success of this symposium

High Temperature Processing Symposium
Swinburne University of Technology
Engineering Building (Hawthorn Campus)

Conference Schedule

Sponsored by Ausmelt, CAST-CRC & Furnace Engineering

Day 1 (8 February 2010) in EN 715

8.30 to 9.00	Registrations in 7th Floor of Engineering Building
Session 1	**Chaired by Professor Geoffrey Brooks (SUT)**
9.00 to 9.10	Welcome by Professor John Beynon, SUT
9.10 to 9.40	01 – **Keynote Speaker**: Professor Oleg Ostrovski, UNSW, Ore Characterisation, Smelting and Reduction in Production of Manganese Alloys
9.40 to 10.00	02 – Professor Doug Swinbourne, RMIT, Modelling Duplex Stainless Steelmaking by the EAF/VOD Route
10.00 to 10.20	03 – Ms Neslihan Dogan, SUT, Kinetics of Decarburisation Reaction in Oxygen Steelmaking Process
10.20 to 10.40	04 – Dr Farshid Pahlevani, Tohoku University, Simulation of Steel Refining Process Parameters on Free Oxygen Content
10.40 to 11.00	Coffee in EN 612
Session 2	**Chaired by Assoc. Professor John Taylor (CAST-CRC, UQ)**
11.00 to 11.30	05 – **Keynote Speaker**: Mr Richard Simpson, Furnace Engineering P/L
11.30 to 11.50	06 – Mrs Barbara Rinderer, Consulting in Partnership P/L, Metal Quality a Key in Aluminium Alloys
11.50 to 12.10	07 – Mr Michael Walton, RefMet, Refractories; an Essential Evil
12.10 to 12.30	08 – Mr Ross Baldock, Ausmelt P/L, Industrial Operation of JAE Nickel Smelting Technology at Jinchuan Nickel Smelter
12.30 to 1.30	**Lunch in EN 612 (Sponsored by Ausmelt, CAST-CRC and Furnace Engineering)**
Session 3	**Chaired by Mr Andrea Fontana (One Steel)**
1.30 to 2.00	09 – **Keynote Speaker**: Dr Paul Cleary, CSIRO, The use of SPH for modelling high temperature flow and solidification applications
2.00 to 2.20	10 – Dr Andrew Campbell, Worsley Parson P/L , Industrial CFD Modelling for High Temperature Processing,
2.20 to 2.40	11 – Mr Morshed Alam, SUT, A Study on Supersonic Coherent Jet Characterstics Using Computational Fluid Dynamics
2.40 to 3.00	12 – Mr Nazmul Huda, SUT, Combustion Modelling of Top Submerged Lance Furnace by Using CFD Tool
3.00 to 3.20	Coffee Break in EN 612
Session 4	**Chaired by Professor Yos Morsi (SUT)**
3.20 to 3.40	13 – Professor Trevor R. Ireland, ANU, High Temperature Processing in the Solar Nebula
3.40 to 4.00	14 – Dr Nawshad Haque, CSIRO, Lifecycle Assessment of Mining and Metal Production
4.00 to 4.40	Panel Discussion – The Impact of Carbon Trading on the Australian Metallurgical Industry

Close of Day 1

Day 2 (9 February 2010) in EN 515

8.30 to 9.00	Registrations in 5th Floor of Engineering Building
Session 5	**Chaired by Mr Robert Matusewicz (Ausmelt P/L)**
9.00 to 9.30	15 – **Keynote Speaker**: Assoc. Professor Brian Monaghan, University of Wollongong, Some Comments on the Study of Metallurgical Coke and Its use in the Iron Blast Furnace: Understanding Process Fundamentals Through Laboratory Studies
9.30 to 9.50	16 – Dr Guangqing Zhang, UNSW, Blast Furnace Ironmaking with Low Coke Consumption
9.50 to 10.10	17 – Mr Jacob Wood, Ausmelt, Large Scale Copper Smelting Using Ausmelt TSL Technology at the Tongling Jinchang Smelter
10.10 to 10.30	18 – Miss Lidya Paulina, RMIT, Distribution of Bismuth between Copper and FeO_x-CaO-SiO_2 slags at 1300°C
10.30 to 11.00	Coffee Break in EN 612
Session 6	**Chaired by Dr Marcus Zipper (CSIRO)**
11.00 to 11.30	19 – **Keynote Speaker**: Professor John Chen, University of Auckland, Physical Model Studies of Some Metallurgical Processes
11.30 to 11.50	20 – Dr Xiaodong Xu, SUT, Online Analysis of Bubble Flow in Metallurgical Operations
11.50 to 12.10	21 – Mr Jiang Chen, University of Queensland, Factors Affecting Nickel Extraction from the reduction Roasting of Saprolite ore in the Caron process
12.10 to 12.30	22 – Dr Robert McNaughton, CSIRO, Development of a High Solar Flux Facility at CSIRO for High Temperature Processes
12.30 to 1.30	**Lunch in EN 612 (Sponsored by Ausmelt, CAST-CRC, and Furnace Engineering)**
Session 7	**Chaired by Dr Akbar Rhamdhani (SUT)**
1.30 to 1.50	23 – Dr Graeme Snook, CSIRO, Application of Current Pulse Techniques to Analysis of Anode Gas Film Behaviour in a Hall Heroult Cell
1.50 to 2.10	24 – Mr Reiza Mukhlis, SUT, Sidewall Materials for Hall Heroult Process
2.10 to 2.30	25 – Ms Vivien Singleton, UNSW, Oxidised Ni-Based Anodes for Aluminium Electrolysis: The Protective Role of the Oxide
2.30 to 2.50	26 – Dr Xiao Yong Yan, CSIRO, A New Route for Producing Metal Borides and Carbides
2.50 to 3.10	Coffee Break in EN612
Session 8	**Chaired by Professor Doug Swinbourne (RMIT)**
3.10 to 3.30	27 – Dr Hector Henao, University of Queensland, Construction and Application of Phase Diagrams for High Temperature Processing
3.30 to 3.50	28 – Mr Behrooz Fateh, SUT, Visualisation of Aluminium Initial Stage Oxidation
3.50 to 4.10	29 – Ms Winny Wulandari, Kinetics of Silicothermic Reduction of Calcined Dolomite in Flowing Argon Atmosphere
4.10 to 4.30	30 – Mr Guangwei Liu, Major Furnace Australia P/L, Automated Aluminium Siphoning System

Close of Symposium

Campus Map – Swinburne@Hawthorn

Multi-storey car park
All day parking $5.50 Mon–Sat
Open 0730–2230. Enter Wakefield Street

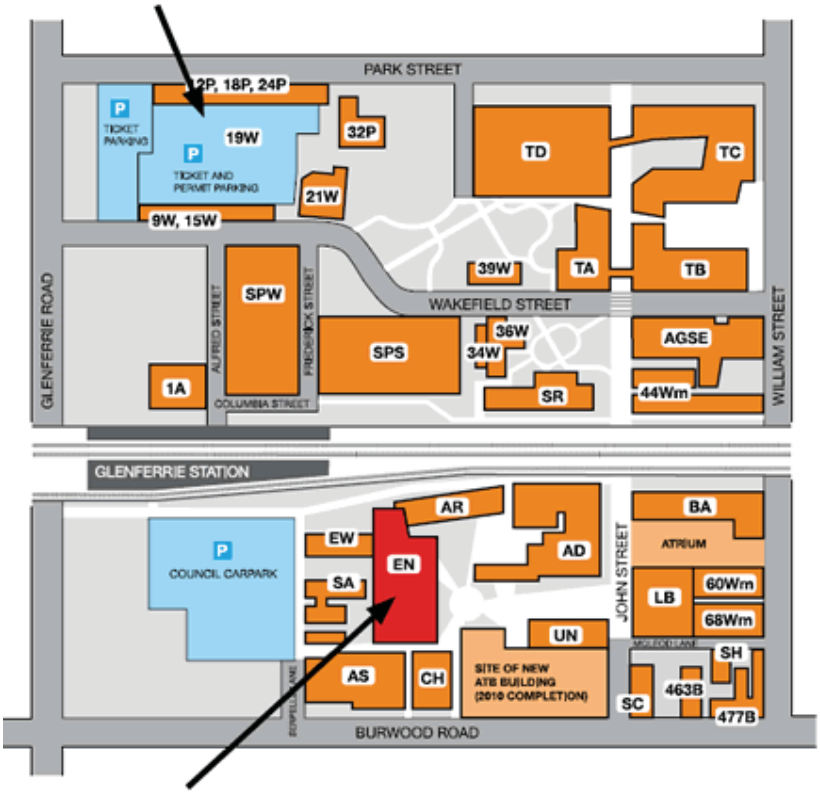

Engineering Building (EN)
Enter via east door

ORE CHARACTERISATION, SMELTING AND REDUCTION IN PRODUCTION OF MANGANESE ALLOYS

Oleg Ostrovski
School of Materials Science and Engineering, University of New South Wales

Keywords: ferroalloys, manganese ore, mineralogy, smelting, reduction

The paper discusses mineralogy of manganese ores, their smelting and reduction in conventional production of manganese alloys, and solid state carbothermal reduction reactions.

1) Phase compositions of manganese ores and their change in the process of calcinations [1,2].

Wessels and Groote Eylandt manganese ores were examined at the University of New South Wales using XRD, optical, SEM and EPMA analyses; CVRD and Gabonese ores were studied at SINTEF and NTNU (Norway) using quantitative XRD analysis. The manganese ores had significant differences in chemistry (Table) and mineralogy. Equilibrium phases in ores at temperatures of 800°C, 1000°C and 1200°C in different gas atmospheres were examined using FACTSage software. The calculated phase composition was in agreement with quantitative XRD analysis. In the process of calcination of manganese ores in air, MnO_2 was reduced to Mn_2O_3 and Mn_3O_4, while during calcination in a reducing atmosphere manganese oxides were reduced to MnO and iron oxides to metallic iron. Formation of a liquid slag in ores at equilibrium was predicted for Wessels, Groote Eyland and Gabonese ores at 1200°C in air and 1000-1200°C in a reducing atmosphere. No liquid slag was predicted for equilibrium phases in CVRD ore.

Table I - Chemical composition of manganese ores

Ore	Chemical composition, wt%							
	MnO	FeO	SiO_2	Al_2O_3	CaO	MgO	BaO	K_2O
Wessels	70.0	14.4	4.18	1.51	8.34	0.73	0.82	-
Groote Eylandt	81.9	5.80	6.09	3.90	0.18	<0.1	0.49	1.53
CVRD	66.0	12.9	9.01	10.3	0.21	0.36	0.24	0.97
Gabonese	83.1	2.68	5.85	7.1	0.08	<0.01	0.22	0.93

2) Ore melting and reduction in silicomanganese production [3].

The charge for silicomangansese production consists of manganese ore, often mixed with ferromanganese slag, dolomite or calcite, quartz and in some cases other additions. These materials have different melting properties, which have a strong effect on reduction and smelting reactions in the production of silicomanganese alloy. The melting and reduction temperatures of different manganese sources were measured in a carbon monoxide atmosphere using the sessile drop method and a DTA/TGA (SINTEF). Equilibrium phases were analysed using FACTSage software. Experimental

investigations and analysis of equilibrium phases revealed significant differences in the melting behaviour and reduction of different manganese sources. The difference in smelting of CVRD ore and CVRD sinter was attributed to faster reduction of sinter by the graphite substrate and carbon monoxide. Calculation of equilibrium phases in the process of reduction of manganese ores using FACTSage correctly reflects the trends in the production of manganese alloys. The temperature at which the manganese oxide concentration in the slag was reduced below 10 wt pct can be assigned to the top of the coke bed in the silicomanganese furnace. This temperature was in the range 1550-1610°C.

3) Solid state carbothermal reduction of manganese oxides [4-6].

Carbothermal reduction of pure MnO to manganese carbide Mn_7C_3 under standard conditions (P_{CO}=1 atm) starts at 1340°C. In industrial production of manganese alloys, manganese oxide is reduced from molten slag. When the MnO content in the slag decreases below saturation level, the reduction is slow and incomplete. Manganese ores start to melt at relatively low temperatures, below 1200°C (depending on the ore chemical composition); carbothermal reduction at temperature of 1200°C is possible at decreased CO partial pressure; equilibrium CO partial pressure for reduction reaction at this temperature is 0.167 atm. Reduction/prereduction of manganese ore in the solid state can be a significant step towards improving overall efficiency of production of manganese alloys.

Non-isothermal and isothermal carbothermal reduction of Groote Eylandt and Wessels manganese ores was studied in hydrogen, helium, argon and hydrogen-carbon monoxide atmospheres. Reduction experiments were conducted in a fixed bed reactor in a vertical tube furnace, with on-line monitoring of gas composition by the CO-CO_2 infrared sensor. The extent of reduction was calculated using the off-gas composition and oxygen content in the reduced samples measured by LECO. The reduced samples were analyzed by XRD and EPMA. Reduction of manganese ores was strongly affected by temperature and ore chemistry. In all gas atmospheres, the reaction rate increased with increasing temperature. The reduction rate of manganese ore in hydrogen was higher than in helium, and in helium higher than in argon. Rate and extent of reduction of Wessels ore were higher in comparison with Groote Eylandt ores.

Acknowledgements
Groote Eylandt and Wessels ores were studied at UNSW with former PhD students M. Yastreboff and R. Kononov. A study of CVRD and Gabonese ores was undertaken at SINTEF (Norway) with involvement of Drs B Sorensen, S Gaal, E Ringdalen, and M Tangstad.

References
[1] R. Kononov, O. Ostrovski, S. Ganguly, Carbothermal solid state reduction of manganese ores: 1. Manganese ore characterisation, *ISIJ International*, **49**, 1099-1106, 2009.
[2] B. Sorensen, S. Gaal, E. Ringdalen, M. Tangstad, R. Kononov, O. Ostrovski, Phase compositions of manganese ores and their change in the process of calcinations. *International Journal of Minerals Processing*, accepted.
[3] E. Ringdalen, S. Gaal, M. Tangstad, O. Ostrovski, Ore melting and reduction in silicomanganese production. *Metallurgical and Materials Transactions B*, accepted.

[4] R. Kononov, O. Ostrovski, S. Ganguly, Carbothermal reduction of manganese oxide in different gas atmospheres. *Metallurgical and Materials Transactions B*, **39B**, 662-668, 2008.
[5] R. Kononov, O. Ostrovski, S. Ganguly. (2009) Carbothermal Solid State Reduction of Manganese Ores: 2. Non-isothermal and Isothermal Reduction in Different Gas Atmospheres. *ISIJ International*, **49**, 1107-1114, 2009.
[6] R. Kononov, O. Ostrovski, S. Ganguly, Carbothermal Solid State Reduction of Manganese Ores: 3. Phase Development. *ISIJ International*, **49**, 1115-1122, 2009.

MODELLING DUPLEX STAINLESS STEELMAKING BY THE EAF/VOD ROUTE

Prof. Doug Swinbourne
RMIT University, Melbourne

Stainless steels are widely used alloys favoured especially for their resistance to corrosion. This resistance is a result of their high chromium contents (~18 wt%), but also requires that they have very low carbon contents (<0.05 wt%). This simultaneous need for high chromium and very low carbon contents causes major difficulties for the steelmaker. Carbon is removed from molten steel by oxidation, but chromium is also very readily oxidized so decarburisation inevitably results in large losses of expensive chromium to the slag.

The competitive oxidation of chromium and carbon has been described by the following reaction;

$$2Cr + 3CO(g) = 2CrO_{1.5} + 3C$$

although there is strong evidence that CrO also forms. Assuming that the carbon monoxide partial pressure is 1 atm., that the slag is saturated with $CrO_{1.5}$ and taking acceptable values for the activity coefficients of Cr and C in molten steel, the equilibrium contents of Cr and C in steel as a function of temperature can be calculated. It can be seen that at 0.05 wt%C and a typical temperature of 1650°C only about 4 wt% Cr can be in the steel. In traditional steelmaking practice in an electric arc furnace this meant that little cheap stainless steel scrap could be used in the charge, and that the required final chromium contents had to be achieved through large additions of very expensive extra-low carbon ferrochromium.

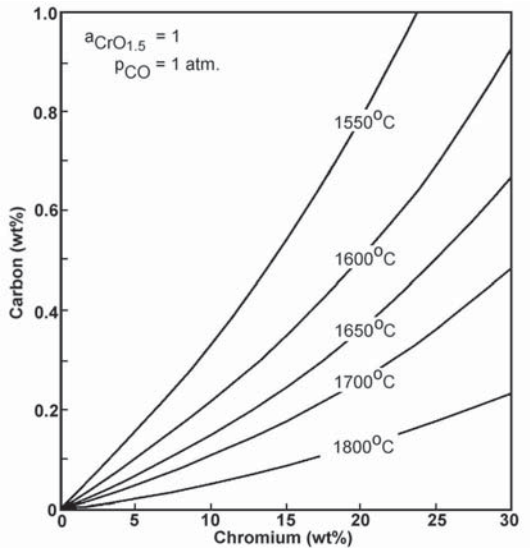

Figure 1 – Cr-C equilibrium in molten steel

In the 1960's it was recognized that reducing the carbon monoxide partial pressure was a very effective way of increasing the equilibrium content of chromium at any carbon content. This was not possible in the EAF, but was possible in a converter by either diluting the oxygen injected with an inert gas (the AOD process) or operating the converter under a partial vacuum (the VOD process). This led to the

development of "duplex processes" in which a relatively high carbon steel melt containing about 18 wt% Cr was produced in an EAF, then decarburized to the required low carbon contents in a converter. In this work the chemistry of the VOD process will be modeled to show how dramatically the system pressure influences the relative extents of chromium and carbon oxidation.

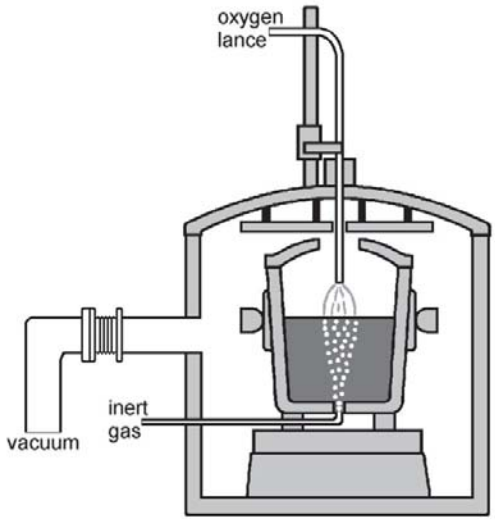

Figure 2 – A typical VOD installation

VOD processing entails holding molten steel in a ladle within a vacuum chamber and injecting oxygen through a top-blowing lance. A small flow of bottom-stirring argon is also required. Oxygen is initially blown onto the melt, with dolomite and lime as fluxes to form a basic slag to protect the basic refractories and achieve desulphurisation. During this time the total pressure is 10 to 20 kPa. The total pressure is then reduced to 100 - 500 Pa without any additions of oxygen, fluxes or ferroalloys. Finally ferrosilicon is added as a reducing agent for the small amounts of chromium oxide that have reported to the slag.

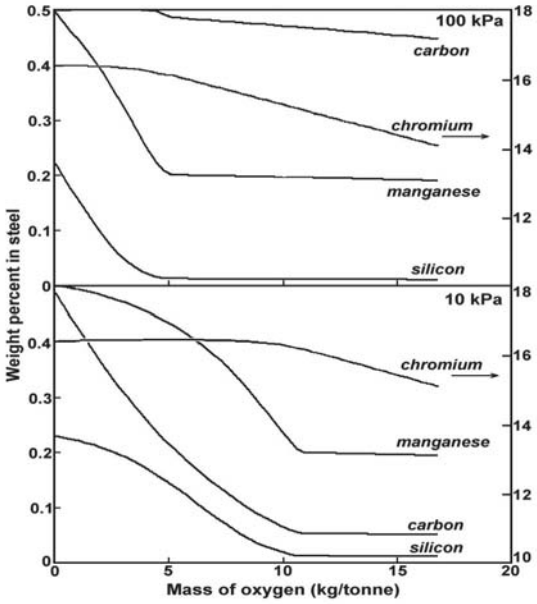

Figure 3 – Concentration of elements in steel

The computational software package "HSC Chemistry for Windows" was used to model the progress of a VOD heat, using activity coefficients calculated by the Ban-Ya RSM model. The HSC database doesn't contain CrO(l) so data for this species was added. Figure 3 shows the concentration of various elements in the steel at both atmospheric pressure (100 kPa) and at 10 kPa during oxygen blowing. The temperature was taken to be 1600 ^{o}C, although it can rise to almost 1800 ^{o}C by the end of the oxygen blow. This temperature rise makes little difference to the predictions made by the model. At 100 kPa little carbon is oxidised while the chromium content drops significantly. At 10 kPa carbon is reduced to a very low level while chromium remains unoxidised until about 10kg O_2/tonne. At this point the small mass of slag present has become saturated with $CrO_{1.5}$ and further blowing creates more solid $CrO_{1.5}$.

The second stage in the VOD is often called "deep degassing" and takes advantage of the fact that the lower the total pressure the lower the CO partial pressure, and therefore the lower the equilibrium carbon content of the steel. Figure 4 shows that lowering the total pressure to 100 Pa (0.1 kPa). The carbon content of the steel is predicted to drop to about 5 ppm. At such low carbon contents the rate of the decarburisation reaction becomes mass transfer limited and equilibrium cannot be achieved without unacceptably long periods of bottom stirring with argon. Most stainless steels only call for carbon contents of 0.02 to 0.05 wt% and this is readily achieved.

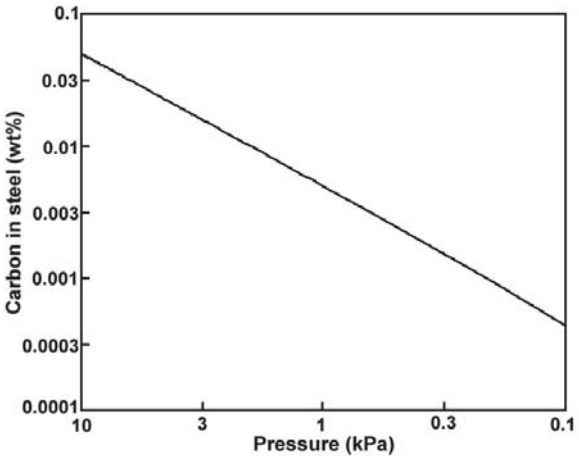

Figure 4 – Carbon content of steel during deep degassing

The final stage of the VOD involves the addition of ferrosilicon to the ladle, the intended reaction being;

$$Si + 4/3\ CrO_{1.5} = 4/3\ Cr + SiO_2$$

Figure 5 shows that solid $CrO_{1.5}$ is first reduced, then $CrO_{1.5}$ and CrO in slag are very significantly reduced. However, as the extent of chromium recovery increases the silicon content of the steel markedly increases. This shows that the efficiency of silicon additions drops, so almost complete recovery of chromium from the slag is impractical.

The trends predicted by the model quite closely reflect those seen in practice. This shows that computational thermodynamics modelling using HSC is a very effective way to gain an understanding of stainless steelmaking practice.

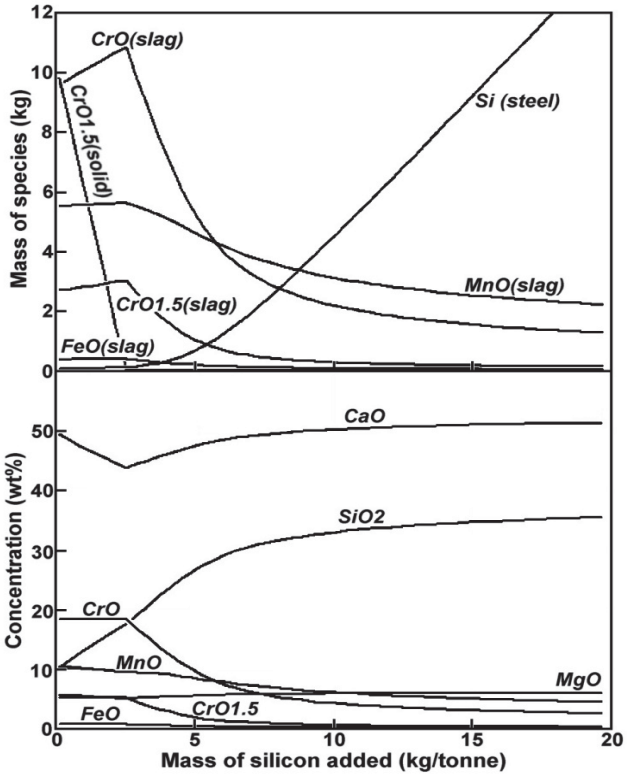

Figure 5 – Changes in composition during reduction.

KINETICS OF DECARBURIZATION REACTION IN OXYGEN STEELMAKING PROCESS

Neslihan Dogan, Geoffrey A. Brooks and Muhammad A. Rhamdhani
Swinburne University of Technology, Hawthorn, VIC 3122 Australia

Key words: global model, decarburization, emulsion, oxygen steelmaking, bloated droplet

The steelmaking process is complex since it involves simultaneous multi-phase (solid-gas-liquid) interactions, chemical reactions, heat and mass transfer and complex flow patterns at high temperatures. The transient nature of the process also adds more complexities and the severe operating conditions inhibit the direct measurement and observation of the process. This difficulty can be addressed by developing models, which make it possible to describe the complicated nature of the process itself and to understand the interconnection of important process variables. A global model of oxygen steelmaking focusing on the overall decarburization of the process and including the new bloated droplet theory has been developed.

Decarburization reaction occurs in different reaction zones using various reaction mechanisms. There are two main reaction zones considered in this study, which are bath and emulsion zone. At the impact zone, as top-blown oxygen reaches to the surface of the liquid bath, it reacts with carbon dissolved in the metal and forms a mixture of CO-CO_2 gases as product. Carbon monoxide further oxidized to carbon dioxide. Subsequently, dissolved carbon also reacts with CO_2 simultaneously at this region. The sequence of the decarburization reactions as follows;

$$[C] + \tfrac{1}{2}O_{2(g)} = CO_{(g)} \quad \text{(Eq. 1)}$$

$$[C] + CO_{2(g)} = 2\,CO_{(g)} \quad \text{(Eq. 2)}$$

It is suggested that gaseous diffusion controls the decarburization rate down to the critical level of carbon, where carbon diffusion in liquid phase becomes rate-limiting step. However, some investigators suggested that sulphur has a determining effect on the reaction rate and chemical reaction at the interface also controls the reaction rate. The mixed control mechanism involving both mass transfer in the gas phase and dissociative adsorption of CO_2 was selected to be the rate determining step.

In the case of emulsion zone, it is proposed that FeO supplies oxygen and liberates CO_2. Oxygen then reacts with CO at slag-gas interface and followed by reaction at the metal-gas interface with CO_2 diffusion through the gas halo. CO_2 provides oxygen to react with carbon in the melt. These reactions involve the sequence as below

$$CO_{(g)} + (FeO) = Fe + CO_{2(g)} \text{ (slag surface)} \quad \text{(Eq. 3)}$$

$$CO_{2(g)} + [C] = 2CO_{(g)} \text{ (metal surface)} \quad \text{(Eq. 4)}$$

The overall reaction is

$$(FeO) + [C] = Fe + CO_{(g)} \quad \text{(Eq. 5)}$$

There is no agreement on description of the mechanism of this reaction and also the rate controlling step of this reaction under various operating conditions. In this study, carbon diffusion in the metal droplet was considered to be rate determining step. The total decarburization rate is obtained by the summation of decarburization rates of droplets with various residence times given in (Eq.6). The procedure to calculate the residence time of droplets was taken from the study of Brooks et al.[1] The generated droplets, whose residence time is smaller than given time-step, are returning from the emulsion phase.

$$M_e \frac{dC}{dt} = \frac{\sum_{i=1}^{n} \frac{m_i}{100}\left(C_i^{t+\Delta t} - C_i^{t}\right)}{\Delta t} \qquad \text{(Eq. 6)}$$

where n is number of present droplets in the emulsion, m_i is weight of a single droplet (kg) and C is the carbon content of droplet (mass%). In this model, carbon content of the metal droplet is assumed to be the same as bulk carbon content. The values for C_i are obtained from the mass balance calculation including scrap melting, decarburization reaction in emulsion and at the impact zone.

The global model, which utilises numerical computational technique, has enabled us to predict the carbon content of bulk metal and metal droplets and the rate of decarburization reaction in the emulsion zone and impact zone throughout the blow for a given operating conditions of dynamics and materials additions for a given input conditions, weights, analysis of scrap and hot metal. The outcome of other refining reactions is entered as known variables from the industrial data. At the end of each time step, the new carbon composition can be evaluated, by means of mass transfer equations. It is considered to utilize the updated values from each sub-routine for the next step. The calculation in this model include the submodels kinetics of scrap melting, kinetics of flux dissolution, droplet generation, droplet residence time, decarburization in the emulsion and at the impact zone and offgas generation and temperature profile of the metal and slag phase. The required process data was obtained from the study of Cicutti et al.[2, 3] Several of the submodels such as flux dissolution and droplet generation that form the global model were validated against industrial data and the results have been published.[4, 5]

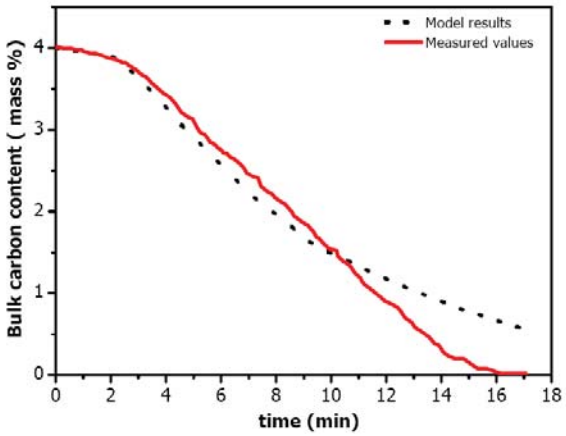

Figure 1 - The comparison of bulk carbon content in metal bath calculated by the global model with the study of Cicutti et al.

Figure 1 shows the comparison of preliminary results of bulk carbon content of the bath as a function of time obtained from the global model with the study of Cicutti et al. It can be seen that the model can predict the change of carbon content well up to approximately two thirds of the blowing period.

The comparison of decarburization reaction in the process predicted by the global model is illustrated in Figure 2. The majority of decarburization during the main blow takes place in the emulsion zone based on the global model. This result is agreement with previous findings[6, 7] that showed that decarburization within the metal droplets dominates the refining of carbon in oxygen steelmaking process. Further optimisations are being carried out especially for the final stage of the blowing, e.g. including the effect of bath stirring.

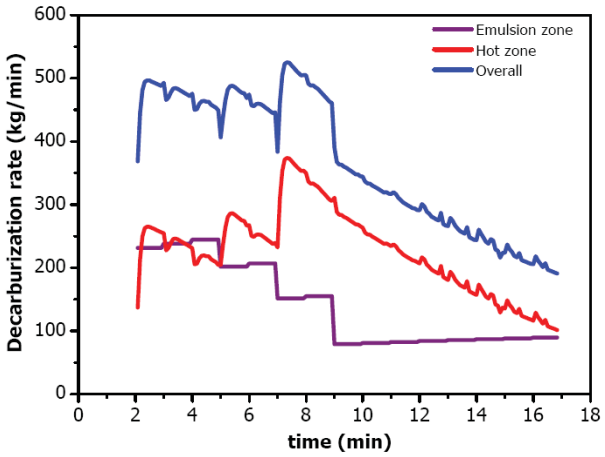

Figure 2 - The comparison of decarburization rates in oxygen steelmaking process calculated by the global model

References:

1. G. A. Brooks, et al., "Modeling of Trajectory and Residence Time of Metal Droplets in Slag-Metal-Gas Emulsions in Oxygen Steelmaking," *Metallurgical and Materials Transaction B*, Vol.36B, No.2005, pp. 525-535.
2. C. Cicutti, et al., "Study of Slag-Metal Reactions in an Ld-Lbe Converter," in 6*th* *International Conference on Molten Slags, Fluxes and Salts*, 2000, City, p. 367.
3. C. Cicutti, et al., "Analysis of Slag Foaming During the Operation of an Industrial Converter," *Latin American Applied Research*, Vol.32, No.3, 2002, pp. 237-240.
4. N. Dogan, G. A. Brooks, and M. A. Rhamdhani, "Analysis of Droplet Generation in Oxygen Steelmaking," *ISIJ Int.*, Vol.49, No.1, 2009, pp. 24-28.
5. N. Dogan, G. A. Brooks, and M. A. Rhamdhani, "Kinetics of Flux Dissolution in Oxygen Steelmaking," *ISIJ In.*, Vol.49, No.10, 2009, pp. 1474-1482.
6. P. Kozakevitch, "Study of Basic Phosphate Slag Foams," International Congress of Oxygen Steelmaking, Le Touquet, 1963.
7. H. W. Meyer, et al., "Slag-Metal Emulsions and Their Importance in Bof Steelmaking," *JOM*, Vol.20, No.1968, pp. 35-42.

SIMULATION OF STEEL REFINING PROCESS IN BOF CONVERTER – EFFECT OF PROCESSES PARAMETERS ON FREE OXYGEN CONTENT

Farshid Pahlevani, S. Kitamura, H. Shibata, N. Maruoka
IMRAM, Tohoku University, Sendai 980-8577 Japan
Contact address: farshid@tagen.tohoku.ac.jp

Keywords: free oxygen content, kinetic model, BOF converter.

There has been a growing interest in the study of the simultaneous dephosphorization in BOF converter. It is usually observed that a partition of elements in the industrial basic oxygen furnace (BOF) in not the same as that at equilibrium. A kinetic approach is necessary for the precise understanding of the reactions occurring in the BOF. To satisfy this requirement, a new kinetic model for the BOF steel making reaction is developed[1)].

In the present work, the basic outline of the model is essentially that of Kitamura et al.[2)] for hot metal dephosphorization but it changed in the way that consider the temperature dependence of various parameters. Also, top-blow oxygen and scrap-melting behavior are taken into account. The modified coupled reaction model governs the interface reaction between slag and hot metal phase. The reacted elements diffused into the slag and hot metal and in slag phase precipitation of dicalcium-Silicate and partition of phosphor was happened. Oxygen which has blown from top lance nozel was considered to react with carbon and Fe and also a part of that consumed as post combustion.

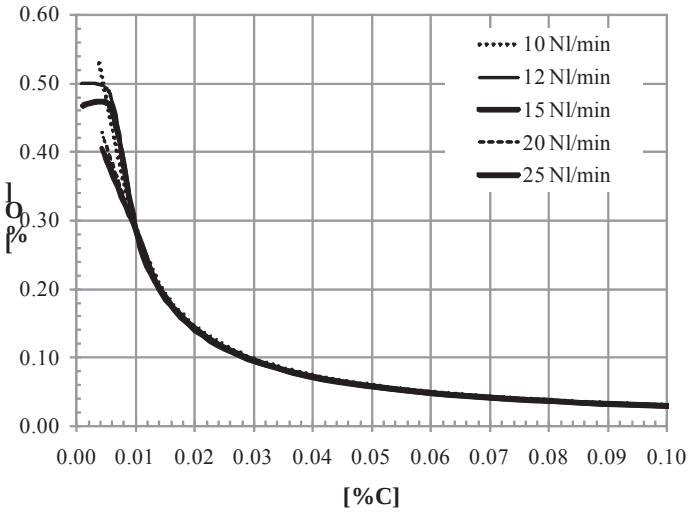

Figure 1 - Effect of Ar-Flow rate on relation between carbon content and free oxygen

To illustrate the usefulness of this approach to the kinetic model of steel refining process in BOF, it was decided to use the model to predict the effect of Ar-flow rate for stirring and oxygen flowing rate on the relation between carbon content and free oxygen in the melt which shown in the figures. At high carbon region amount of free

oxygen will govern by carbon-oxygen reaction. So changing the Ar-flow rate and oxygen supplying rate would not change the amount of free oxygen because of sufficient enough of carbon and reaction between carbon and oxygen. But at low carbon content reaction between iron and oxygen will govern the amount of free oxygen. By increasing the Ar-flow rate the reaction between Fe and free oxygen will increase and amount of free oxygen will decrease (Figure 1). As shown in the Figure 2 by increasing the oxygen flowing rate the amount of free oxygen increases due to constant reaction speed between iron and oxygen.

As a conclusion a kinetic model for the BOF steelmaking reaction has been developed. This model can be used to predict the optimum conditions for dephosphorization in BOF.

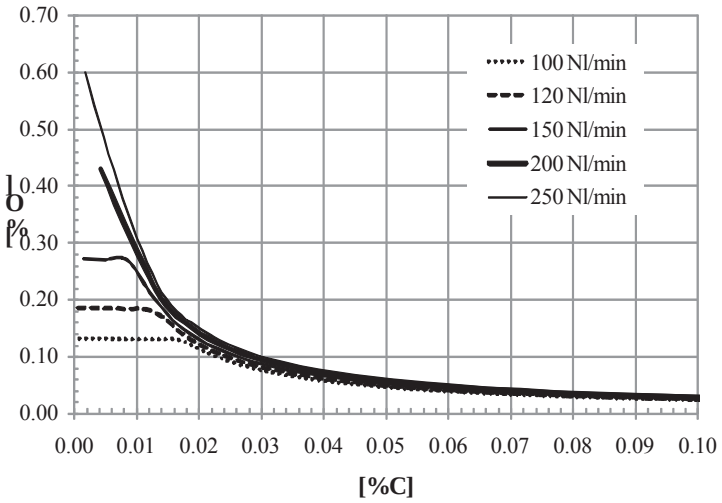

Figure 2 - Effect of O_2 flowing rate on relation between carbon content and free oxygen

References

1. S. Kitamura et al; Proceeding of SCANMET III, p. 283, (2008)
2. S. Kitamura et al; ISIJ International, 49 (2009), p. 1333

METAL QUALITY A KEY IN ALUMINIUM ALLOYS

Barbara Rinderer[1]
[1]Consulting in Partnership Pty Ltd

Keywords: metal cleanliness, cast house operations, molten metal

The metal quality of aluminium alloys is a key concern for the production of extruded and rolled products. From the moment the cast house receives metal from the reduction cell, there are unwanted impurities and inclusions in the molten metal that will be the subject of various processing steps prior to casting. The metal quality must be carefully controlled to meet the property requirements of the alloys undergoing further thermomechanical processing. For example, inclusions can lead to defects such as tearing or surface imperfections and impurities may result in poor mechanical properties. Applications such as thin gauge foil (6 µm in thickness) are very demanding of the metal cleanliness of the cast product.

Molten metal from a primary aluminium smelter may contain inclusions such as cryolite (Na_3AlF_6), or chiolite ($Na_5Al_3F_{14}$), and carbide particles (Al_4C_3) originating from the electrolytic bath used in the Hall Héroult cell (see Figure 1). In addition, the elemental content of the molten metal often does not meet the chemical requirements for the alloy. Thus the cast house will devote considerable effort to the metal cleanliness and control of chemistry related to the incoming metal, aside from other process operations in the cast house.

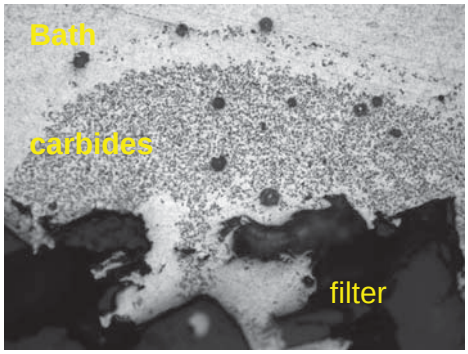

Figure 1 - SEM micrograph shows cross-section of a PoDFA sample collected from a transfer crucible from an aluminium reduction cell. Globular bath particles as well as copious quantities of carbide particles are observed [1].

Application of a flux can assist in improving the metal quality of the molten metal through chemical reaction and floatation where the impurities report to the surface dross layer which can then be removed. Application of a $MgCl_2$/KCl melt refining flux is common. While flux can be added manually, the reaction kinetics are improved by addition using a system such as a rotary flux injector (RFI) in the furnace. The melt processing time is often dictated by the need for control of the sodium concentration. This element is particularly of concern to rolled products due to formation of edge cracking. Levels of only a few ppm are demanded in the cast product for rolling,

compared to ~150 ppm Na in the molten metal from the reduction cell. It is ironic that higher efficiencies in the reduction cell results in higher Na levels.

Flux treating of the crucible before entering the furnace (such as TAC) are used by some operations to reduce the alkali levels. This can be a requirement for operations where molten metal is delivered directly to the customer. Such equipment involves considerable capital investment and it is common to include bath skimming prior to the TAC operation as release of Na into the molten metal occurs as a result of the reaction of bath with Mg from the flux.

$$2\ Na_3AlF_6 + 3\ Mg \Rightarrow 6\ Na + 2\ AlF_3 + 3\ MgF_2 + Al \qquad (1)$$

Additional processing steps may also be introduced in the cast house for the control of bath carry-over and reducing alkali concentration. This includes the use of double transfer where the contents of one crucible are decanted into another to encourage evaporation during the transfer. This is, however, at the expense of oxidation related to turbulence and contributes to additonal melt loss. Some innovations related to addition of flux at the reduction cell during tapping have been proposed (Icon system [2]), but have not yet been commercialised. Other work has been in the area of improved tapping operation at the reduction cell in an attempt to avoid bath carry-over [3]. For high quality products, alkali control will require multiple processing steps; TAC, RFI and further degassing during the casting operation to meet the product requirements.

Practices for control of inclusions begin with furnace operations related to stirring, settling and management of dross in the furnace. The rapid oxidation of aluminium will result in the generation of oxide films in any turbulent operation such as furnace filling. Siphoning into the furnace will greatly impact on minimisation of dross, but conversely the sodium content of the metal is higher with this transfer compared to tipping. Dross at the surface can be scrapped off, but there is considerable aluminium metal also trapped in the dross layer (up to 80% Al metal). While careful practices to avoid thermiting and erosion of the metal content will be beneficial along with dross reprocessing, the cost associated with dross formation is substantial.

As a final control of inclusions there is the use of filtering, although this is not 100% efficient. There are different technologies currently available including ceramic foam filtration (CFF) consisting of an alumina structure which allows capture of inclusions both within the filter through impingement and through cake filtration at the filter entry. As metal cleanliness demands increase for critical products, other filter technologies such as deep bed filter (DBF) or porous tube filtration (PTF) are often favoured.

Other metal cleanliness concerns in smelter metal may be related to the raw materials source. Fine alumina particles may not be converted in the reduction cell and can result in undissolved alumina being transferred to the cast house. This has been associated with “sludgy” metal and the premature blocking of filters (Figure 2). Many of the impurity elements in the smelter molten metal are directly related to the raw material chemistry. Low iron content alumina may be particularly sought for metal destined for high purity applications and some foundry applications. Cell control will also be a factor as iron can also be released into the molten metal from the cast iron anode rods. In addition, the carbon anode composition also impacts the molten metal chemistry. Rising Ni and V levels in coke impacting on aluminium alloys has been noted as a looming issue [4].

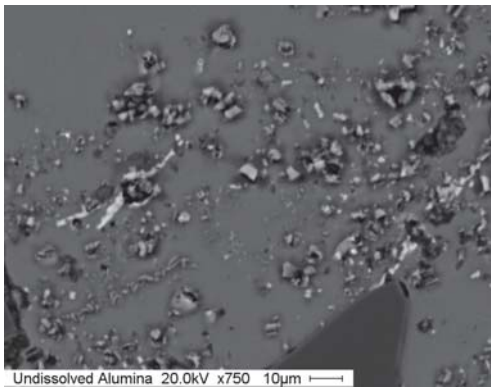

Figure 2 - SEM micrograph from a spent filter illustrates undissolved alumina particles originating from the reduction cell [1].

The impact of the reduction cell operation on the molten metal quality and the need for subsequent cast house operations has been discussed. With a global focus on environmental emissions and energy consumption, production of primary aluminium is receiving particular attention. Energy reduction initiatives or potential new cell technologies will also require attention to the control of impurities and inclusions in molten metal and their management in the cast house.

References

[1] P.R. Austen, The Need for Process Control from Raw Material to Cast Product, *Aluminium Cast House Technology XI*, Gold Coast, 2009

[2] E. Aspen, B.A. Heggset, J.H. Vaagland, ICON-Pre-treatment of pot-room metal, *Light Metals 2008*, TMS, p577, 2008

[3] V. Goutiere, C. Dupuis, Understanding the Mechanisms of Bath Carry-Over with Molten Aluminium in Smelters, *Light Metals 2008*, TMS, p563, 2008

[4] J.F. Grandfield, J.A. Taylor, The Impact of Rising Ni and V Impurity Levels in Smelter Grade Aluminium and Potential Control Strategies, *Materials Science Forum*, **630**, p129, 2009

REFRACTORIES; AN ESSENTIAL EVIL?

Michael C. Walton
RefMet, Melbourne

Keywords: Refractories; Compatibility, Longevity

1. Introduction

The high temperature processing industry depends almost entirely on Refractories. For process vessel integrity and longevity, it is essential to choose the appropriate refractory lining, or the opportunity costs in lost production and unproductive time can be immense. Unfortunately, many operators do not have a sufficient understanding of the topic to make informed decisions, and often rely on suppliers recommendations, with mixed results.

This presentation focuses on the main decision factors in choosing an appropriate material for the lining of a vessel, and some general decision factors to assist in obtaining a successful outcome in the process environment.

2. Compatibility Factors

2.1 Temperature

The most obvious factor is operating temperature. The refractory must be chosen so it has 'head-room on temperature to accommodate the inevitable process fluctuations. The chart below indicates the range of some common processes.

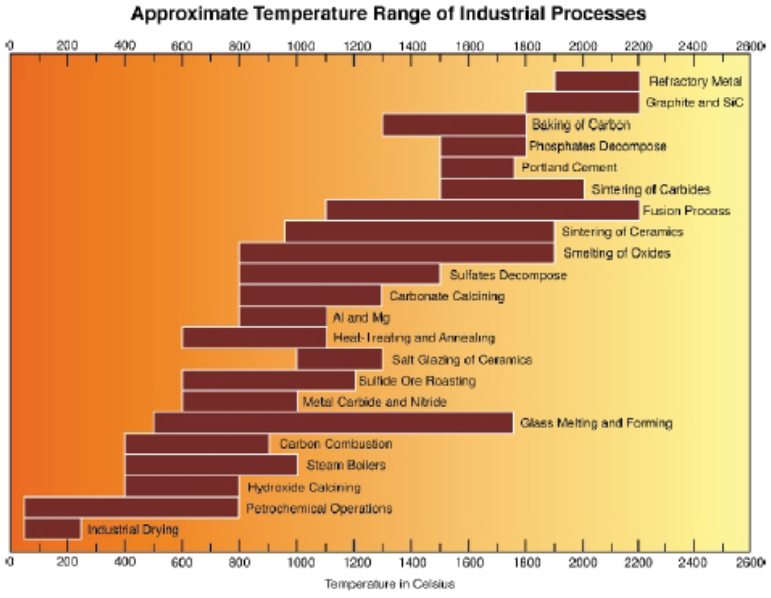

Temperature regimes for industrial applications of refractories.

But not only is operating temperature important, but so is the likely temperature variation, and how quickly this may happen (Process spikes!).

2.2 Slag Chemistry

In processes where there is a separation of liquid phases (i.e. Smelting), one of the most important factors is the compatibility of these phases with the vessel lining. As most liquid metals are not too reactive, this boils down to the slag make. Incompatibility is the major source of high temperature erosion/corrosion of refractories at high temperatures.

The figure below is a good starting point to assess compatibility of slags to various types of refractories.

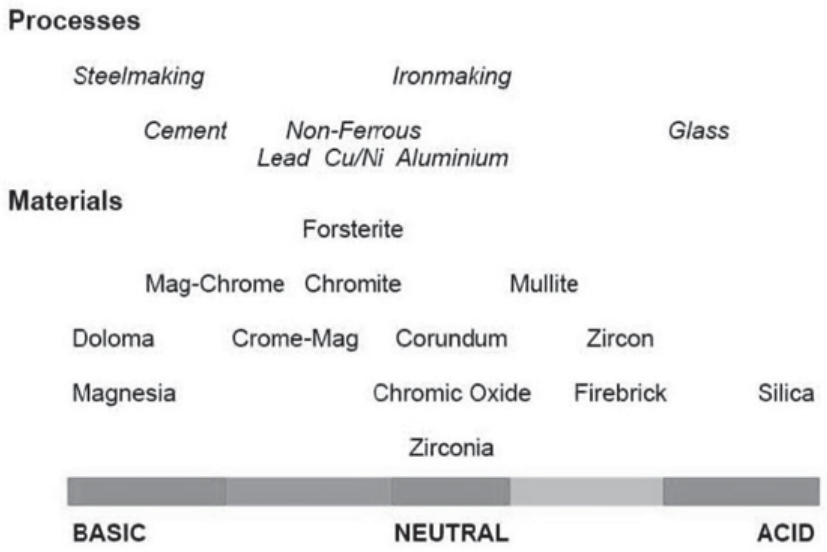

2.3 Chemical action

While I have said above that most liquid metals are relatively inactive, there are some that are. For example, the most pervasive is Aluminium, and this causes issues with alumino-silicate refractories, with its ability to reduce the free silica in the material to silicon, and thus destroy the refractory matrix, and deposit Corundum.

$$4Al + 3SiO_2 = 2Al_2O_3 + 3Si$$

To avoid this, materials have to be carefully chosen, and often dosed with other chemical species to retard this reaction.

Another major chemical problem is the reaction between reducing carbonaceous gases (e.g CO) and ferric oxide which may be present in the refractory as a contaminant. The reaction deposits elemental carbon in the refractory structure causing surface bursting.

$$Fe_2O_3 + 2\,CO = 2FeO + CO_2 + C$$

Similar issues exist with mattes (metal sulphides) and Chlorides, both liquid and gaseous.

2.4 Mechanical Issues

It seems reasonable to expect refractories to mechanically fail when overstressed. However, it is often overlooked that they do not behave like steel. They are strong only in compression, and generally do not have a 'softening' point, but fail rapidly if only slightly overheated. They also have different elastic (E) properties. This can usually be accommodated in the design stage provided accurate process information is provided for calculation of the following parameters:

- Thermal expansion
- abrasive component (dust laden high velocity gases)
- Bending moments
- Auxiliary anchoring systems (stainless steels/alloys)

3. Overview

The design of a suitable system is complex, as there is unlikely to be one material to adequately cover all the issues adequately. Thus Zoning may be necessary. I will illustrate this by reference to a cement kiln, where the critical type of stress varies at different areas of the kiln. We will consider:

- Thermal stress
- Mechanical stress, and
- Chemical stress

Thermal stress is worst in the area near the burner at the discharge end of the kiln, where the temperatures can be up to 1600ºC. Mechanical stresses are most severe over the tyres and gears spaced along the kiln. Chemical stresses are worst where the liquid phases are formed, and the calcination reactions take place-called the burning zone; and also where the sulphates and alkalis deposit.

If we put these together on an 'indexed' chart (upper illustration) against kiln length (lower), we arrive at the figure below, where Green is maximum chemical stress, Blue is thermal and Red is mechanical. This leads to application of different refractory types in different areas to combat these varying factors.

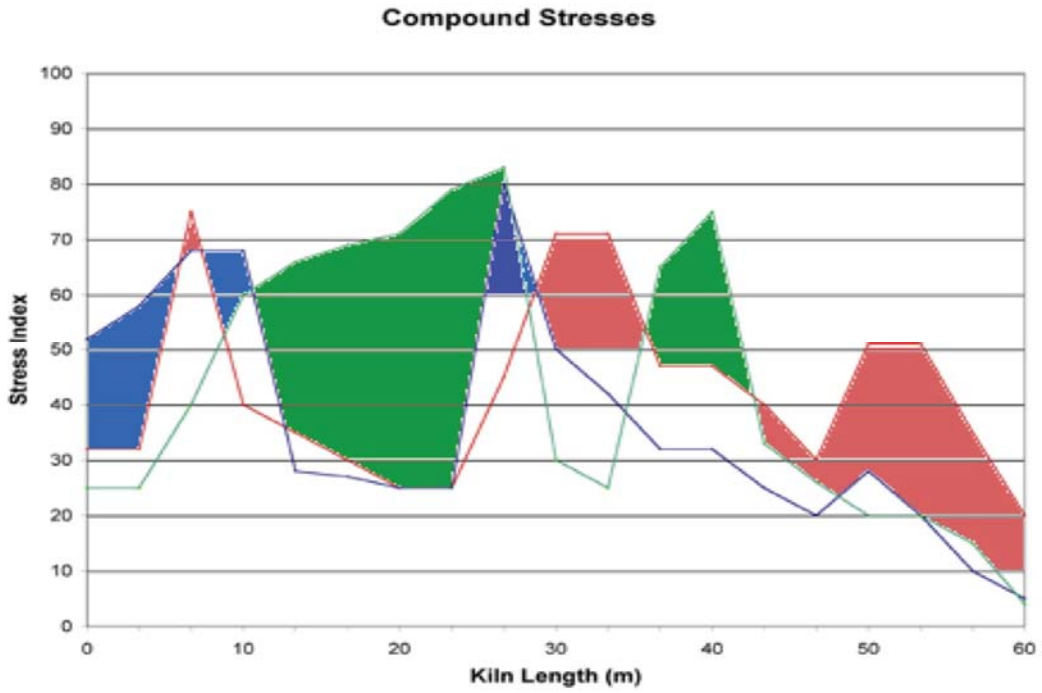
Compound Stresses
Stress Index
Kiln Length (m)
0
10
20
30
40
50
60
70
80
90
100

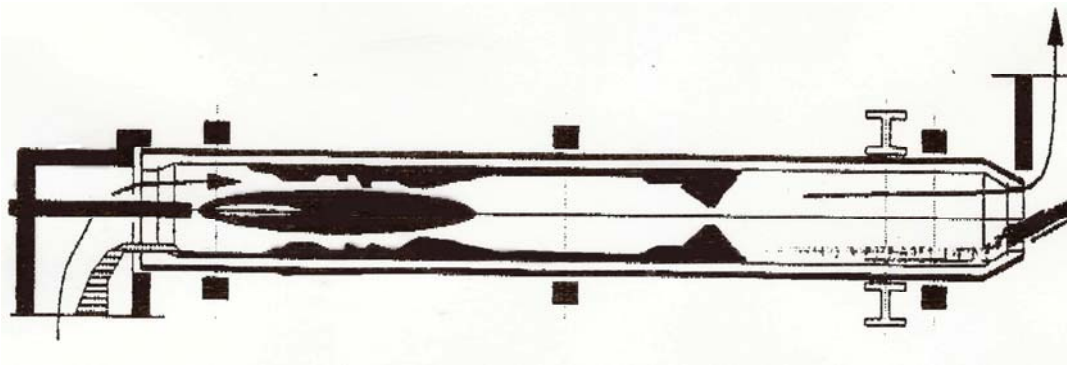

INDUSTRIAL OPERATION OF JAE NICKEL SMELTING TECHNOLOGY AT JINCHUAN NICKEL SMELTER

ZHOU Min[1], WAN Aidong[1], LI Guang[1], Ross Baldock[2] and Harry Li[2]

[1]Jinchuan Non-Ferrous Metals Corporation, People's Republic of China
[2]Ausmelt, 12 Kitchen Rd Dandenong, Victoria, Australia

Key-Words: TSL, Nickel Smelting, Industrial Operation, Nickel

Abstract

A commercial nickel smelter using JAE Nickel Smelting Technology has been successfully commissioned and put into the smooth operation at Jinchuan Non-ferrous Metals Corporation China since August 2008 after 2.5 years of design and construction works. The paper provides details of this nickel smelting project, including the technical evaluation, demonstration plant investigation, engineering design, plant commissioning and operation. Emphasis has been given in comparison between the design targets and actual performance of the plant highlighting the fast ramp-up to full production of this largest Ausmelt TSL furnace to date.

References

[1] T. McNulty, "Developing innovative technology", *Mining Engineering Magazine*, October 1998.
[2] Factsage [1976-2009], Version 6.0, Thermfact and GTT-Technologies. URL: http://www.factsage.com.

THE USE OF SPH FOR MODELLING HIGH TEMPERATURE FLOW AND SOLIDIFICATION APPLICATIONS"

Dr Paul Cleary
CSIRO

SPH is a particle based method that has advantages in modelling flows with any combination of high speed flows, complex free surface motion including splashing, history dependence and phase change. This makes SPH well suited to a range of high temperature applications. The basis of the computational method will be described. Examples in casting (with solidification), pyrometallurgy and combustion will be presented.

INDUSTRIAL CFD MODELLING FOR HIGH TEMPERATURE PROCESSING

Dr Andrew Campbell
Manager CFD Modelling
WorleyParsons Advanced Analysis Group Melbourne

Computational Fluid Dynamics (CFD) modelling provides operators of high temperature processes the opportunity to better understand their processes. It is difficult to perform detailed and accurate process measurements of smelting and other similar processes due to the aggressive environment and the health and safety implications of undertaking a meaningful measurement campaign.

WorleyParsons uses CFD to assist with the analysis of existing process problems and assisting with examining design issues for new or expanded process plants. This presentation will provide an overview of modelling of a smelter offgas system, electric furnace hot gas cooler, and Electrostactic Precipitator in addition to the challenges of providing meaningful and accurate results within commercially practical timeframes.

CFD modelling of a smelter offgas system was used in conjunction with site measurements to develop a model to predict the capture efficiency from the various hoods that make up the system. After validating the model against the collected measurements, the geometry and model was adjusted to assist with increasing the effectiveness of the system.

An electric furnace operator was examining options for increasing the capacity of their offgas system, and a less capital intensive option was to up-rate the existing cooler. As the cooler was not designed to handle the increased rates, a model was developed of the existing cooler and then modifications made to account for increase cooling air were made. The behaviour of the hot particulate matter carried over with the offgas was of particular interest due to accretion and wear issues involved.

An electrostatic precipitator was modelled to examine the char collectors and potential replacement options for the end of life small cyclonic collectors that are existing. The model predicted the particulate capture efficiency through the collectors, along with the flow distribution through the precipitator. This model had particular challenges, in particular the amount of required detail of the collectors, baffles required a significant amount of modelling effort and maintaining the domain within the computational limits available.

A STUDY ON SUPERSONIC COHERENT JET CHARACTERISTICS USING COMPUTATIONAL FLUID DYNAMICS

Morshed Alam, Jamal Naser and Geoffrey Brooks
Faculty of Engineering and Industrial Sciences
Swinburne University of Technology
P.O. Box H-38, Hawthorn, Victoria 3122, Australia
Email: mmalam@swin.edu.au

Supersonic gas jets are widely used in BOF and EAF steelmaking for refining the liquid iron inside the furnace. Supersonic gas jets are preferred over subsonic jets because of high dynamic pressure associated with it which results in higher depth of penetration and better mixing. Laval nozzles are used to accelerate the gas jets to supersonic velocities of around 2.0 Mach number in steelmaking. When a supersonic gas jet exits from a Laval nozzle, it interacts with surrounding environment to produce a region of turbulent mixing. This process results in an increase in jet diameter and decrease in jet velocity with increasing distance from nozzle exit. During oxygen blowing, the higher the distance between liquid surface and the nozzle exit the more is the entrainment of surrounding fluid which in turn decreases the impact velocity as well as momentum transfer to the liquid. Hence, it is desirable to locate the nozzle close to the liquid metal surface. But the disadvantage of this is the sticking of slag/metal droplets on the lance tip which results in poor tip life. In order to solve the problem, coherent jet technology has been introduced in the EAF steelmaking process at the end of last century. The potential core length (the length up to which the axial jet velocity is equal to the exit velocity at the nozzle) of a coherent supersonic jet is about 40 nozzle diameters compared to 10 nozzle diameters in case of normal supersonic jet. Coherent gas jets are produced by surrounding the normal supersonic jet with flame envelope [1]. The flame envelope is created using a fuel and oxidant. Due to the flame, the entrainment of the surrounding gas into the supersonic jet is reduced, leading to a higher potential core length of the supersonic jet. Although the steelmaking industries have been using the coherent supersonic jet for last one decade, not much research work has been done to investigate the physics involved in supersonic coherent jet. In this study, Computational fluid dynamics (CFD) simulations of supersonic jet with and without shrouding flame were carried out and validated against experimental data [2]. The numerical results showed that the potential core length of the coherent supersonic jet is 4 times longer than that of a supersonic jet without flame shrouding which were in good agreement with experimental results. The CFD model results were then used to analyse the flame shrouding effect on the central supersonic jet.

A 2D computational grid was used for the simulation. The numerical simulations were carried out by solving the unsteady continuity, momentum and energy equations. For each species separate scaler equation has been solved. Temperature corrected k-ε turbulence model was used for the modelling of turbulence. The fuel and oxidizing agent used in the present study is CH_4 and O_2. Nitrogen and Oxygen were used as the central supersonic jet. Only one step of reaction has been considered. The equation of reaction is given by,

$$CH_4 + 2O_2 = CO_2 + H_2O$$

Eddy break up combustion model has been used for the modelling of the combustion flame.

Figure 1 shows the velocity distribution of the supersonic jet with and without shrouding effect. The potential core length of the supersonic oxygen jet with shrouding flame is approximately 4 times higher than that without shrouding flame. Again the potential core length of the shrouded supersonic oxygen jet is higher than the potential core length of the shrouded supersonic nitrogen jet. Figure 1 also shows the axial velocity distribution of the shrouded supersonic N_2 jet with flame deflector. Although the CFD results shows that potential core length of the jet increases when flame deflector is used but it still underpredicts the experimental results [2]. Study is going on to understand the reason for this difference.

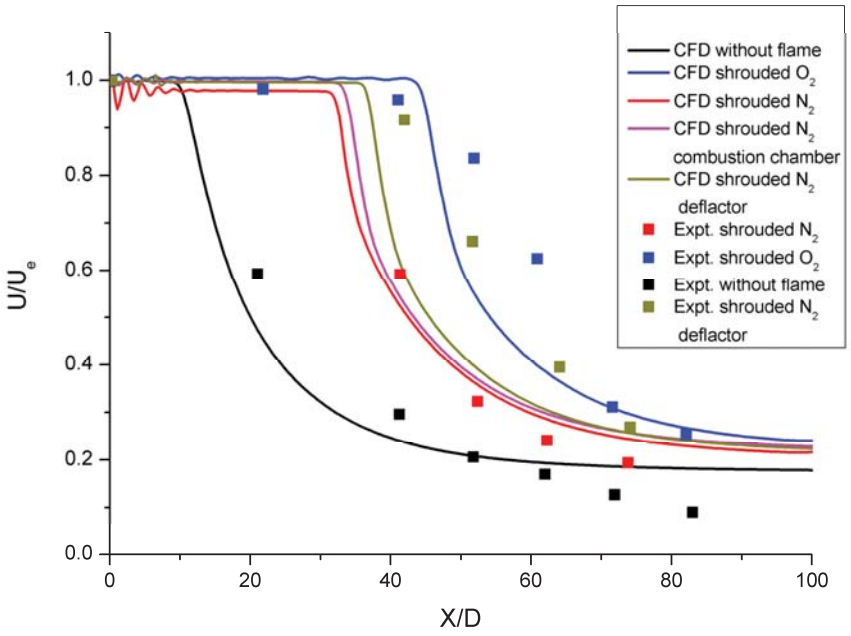

Figure 1

In summary, it can be said that shrouded supersonic jets are very important for steelmaking because it allows the injector to be installed at a distance from the liquid surface which in turn protects the lance tip from corrosion. The present study should allow improved design for shrouded supersonic jet in more effective way.

Reference

1. Sarma *et al. "Fundamental Aspects of Coherent gas Jets"*, Proceedings of the electric furnace conference, ISS, Vol. 56, 1998
2. Anderson *et al*. "*Coherent Gas Jet*" US patent No. 5823762, Oct 20, 1998.

COMBUSTION MODELLING OF TOP SUBMERGED LANCE FURNACE BY USING CFD TOOL

Nazmul Huda[1], J. Naser[1], G. Brooks[1], M. A. Reuter[2], R. W. Matusewicz[2]
[1]Swinburne University of Technology, Hawthorn, Vic 3122, Melbourne, Australia
[2]Ausmelt Limited, 12 Kitchen Rd, Dandenong, Vic 3175, Melbourne, Australia

Top Submerged Lance Technology (TSL) have been successively applied to recovery of a range of metals like tin, lead, copper, zinc, silver, nickel, aluminium, gold etc. around the world. Floyd [1] has described the details of Top Submerged Lance technology and its development since the 1970's.

An investigation of fluid flow into a TSL system to reveal the detail process kinetics in a cold flow water model has been carried out by the present authors [2, 3] by using 3-D Computational Fluid Dynamic modelling technique. As a continuation of that research, a Computational Fluid Dynamic (CFD) model of the high temperature combustion phenomena in a TSL furnace was developed by incorporating the detail chemical reactions involving combustion. In the first stage, a single-phase 3-D combustion model for CH_4 combustion was developed and temperature profile and mass fractions of fuel and air were investigated inside the combustion chamber at the lance tip. Then the model was extended to Multiphase flow simulation of zinc fuming process of a pilot plant with heat, mass, momentum and turbulence interfacial interaction between the phases. The chemical reactions between the slag components and gaseous species were also taken into account.

The pilot plant scale multiphase flow simulation consists of a very complex flow pattern with significant exchange of mass, momentum, energy and turbulence involving complex chemical reaction. A 3D CAD model of the Ausmelt's Pilot plant furnace was developed using CAD tool RHINO. The furnace modelled has a diameter of 0.5 m, length 1.68 m. The generated grid for CFD analysis is shown in Figure 1(a), and the temperature profile of the furnace inside the wall is shown in Figure 1(b). The modelled furnace contained 0.6 m with ISF slag with a composition of *ZnO*, SiO_2 and *FeO* and *CaO* shown by point 'A' in Figure 3. Seven different species were considered for gas phase reaction (CH_4, N_2, O_2, CO_2, CO, H_2O and Zn). Air was injected through the annulus of the lance and CH_4 through the central hole of the lance as the fuel. Air and gas flow rates were kept exactly as the pilot plant trial data.

The simulation results give some interesting insights for complex metallurgical flows and transient concentrations of slag components and gaseous species inside the molten slag bath. Figure 2(a) shows species mass fraction for CH_4 in the combustion chamber at the lance tip and 2(b) shows species mass fraction for CO_2 generated inside the furnace due to combustion. Figure 4 shows zinc loading in the process gases in equilibrium with slag containing 5% zinc taken from Ausmelt's internal report of silver spur slag fuming trials. The CFD results for ISF slag fuming in normal condition is also shown on the same figure. The model is still in the validation phase and some plant trials will be carried out to validate the model.

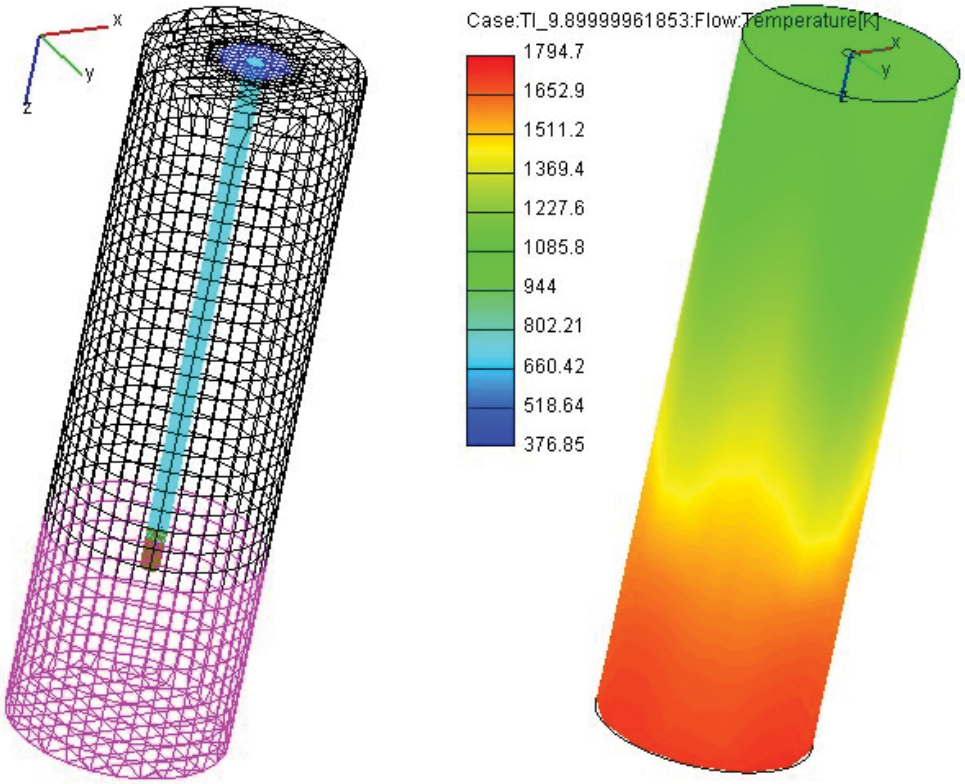

1(a) 1(b)

Figure 1: (a) 3-D view of the generated grid of pilot plant TSL furnace, (b) Temperature profile at the wall inside the furnace

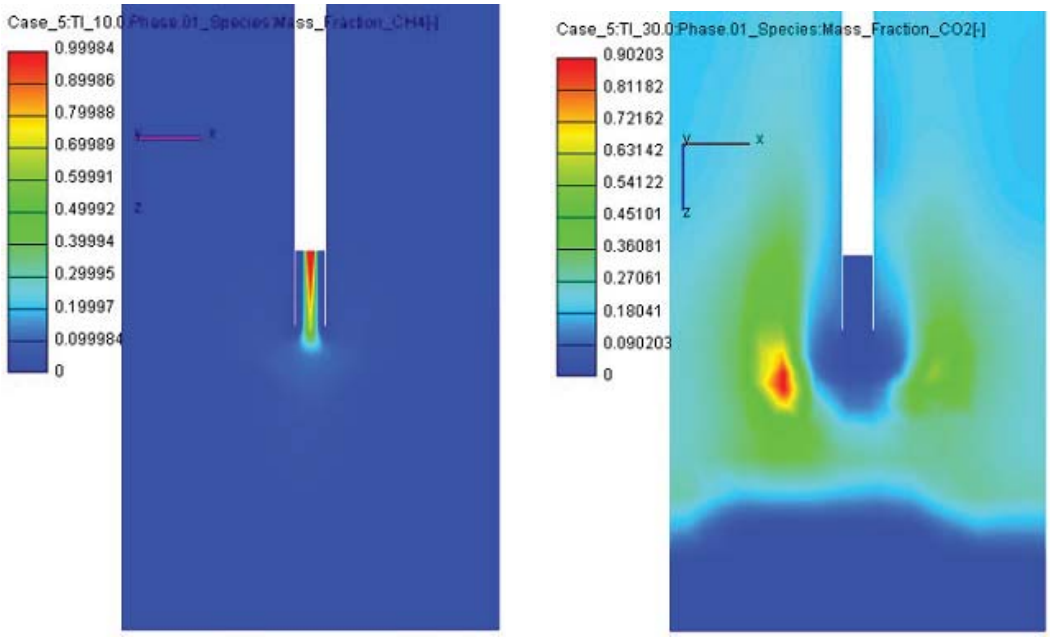

2(a) 2(b)

Figure 2: (a) CH_4 mass fraction in the combustion chamber at the lance tip, (b) CO_2 mass fraction inside the furnace.

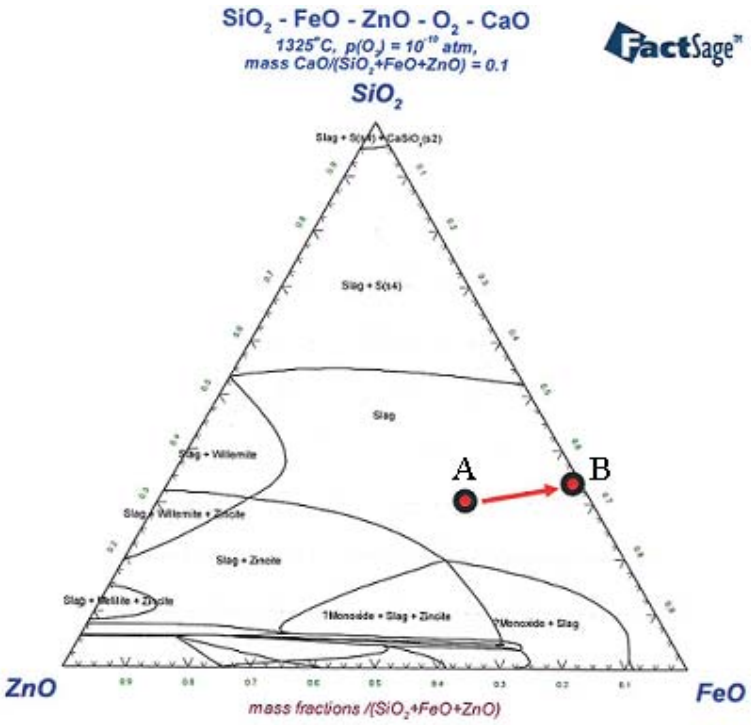

Figure 3: Simplified phase relationships for the reduction step in an Ausmelt furnace for the components *FeO_x*, *ZnO*, *CaO* and *SiO_2*

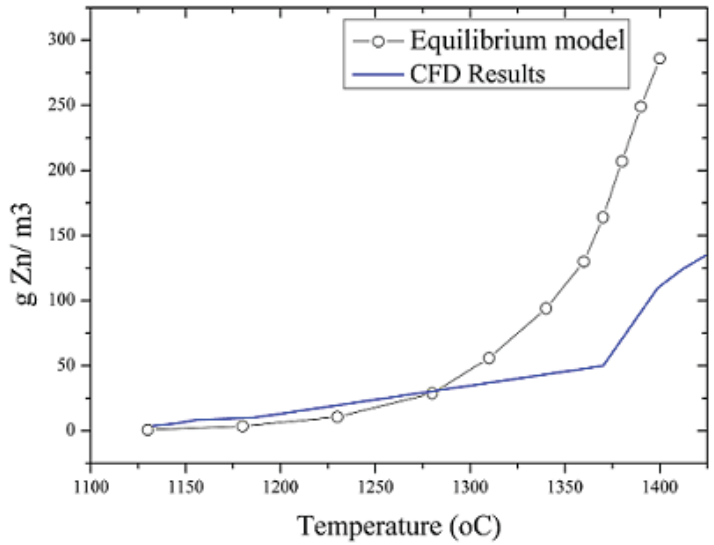

Figure 4: Effect of Temperature on zinc fuming

References:

1. Floyd, J., *Converting an Idea into a Worldwide Business Commercializing Smelting Technology*. Metall. Trans. B., 2005. **36**(B): p. 557-575.
2. Huda, N., et al. *CFD Modelling of Gas Injections in Top Submerged Lance Smelting* in *TMS Annual General Meeting*. 2009. San Francisco, California.
3. Huda, N., et al., *CFD Modeling of Swirl and Non-swirl Gas Injections into Liquid Baths Using Top Submerged Lances* Metall. Trans. B., 2010. **41**(1): p. 35-50.

HIGH TEMPERATURE PROCESSING IN THE SOLAR NEBULA

Trevor R. Ireland[1],
[1]Research School of Earth Sciences, The Australian National University,
Canberra ACT 0200

Keywords: volatility, fractionation, Solar Nebula, meteorites

Our solar system evolved from a cold molecular cloud into the ordered and structured solar system we see today. The earliest record from the solar system shows the separation of the elements (fractionation) because of different affinities. Many of these fractionations occur today in the Earth as magmas crystallize and separate. However some of the processes in the early solar system occurred at extremely high temperatures causing fractionation of elements that are often regarded as ultrarefractory.

Such fractionations are most pronounced in the lanthanides or rare earth elements whose terrestrial relative abundances are typically governed by ionic size, producing smooth variations in abundance-normalised plots. In refractory inclusions in meteorites, these patterns can be quite different with one common pattern showing depletions in the ultrarefractory REE (Gd-Er and Lu), while Tm has an abundance similar to the lighter REE[1]. Such a pattern has been ascribed to removal of an early ultrarefractory component prior to condensation of the remaining gas. However, such behaviour cannot be predicted from relevant thermodynamic data and represents a major shortcoming in our ability to accurately discern between volatility-controlled condensation records versus liquid–controlled fractionation of elements between crystallizing phases.

We are looking to replicate the high temperature conditions in an experimental apparatus for which we can measure abundance fractionations and determine relevant thermodynamic data. In this way we hope to determine the physicochemical environment governing the high-temperature fractionation and place the formation of refractory inclusions in an appropriate astrophysical context.

References

[1] T. R. Ireland, B. Fegley Jr, The solar system's earliest chemistry: Systematics of refractory inclusions. *Int. Geological Review* **42**, 865-894, 2000.

LIFE CYCLE ASSESSMENT OF MINING AND METAL PRODUCTION

N. Haque, T. Norgate
CSIRO Minerals Down Under Flagship
Box 312, Clayton South, VIC 3168

The life cycle of a product or a process system covers the consecutive and interlinked stages from raw material acquisition or generation from natural resources to final disposal. Life cycle assessment (LCA) studies of mining, mineral processing and metal production have been carried out at CSIRO Process Science and Engineering in recent years (Norgate and Haque, 2010; Norgate *et al*., 2007). These studies have included iron and steel, copper, nickel, aluminium, lead, zinc and titanium, both by pyro-metallurgical and hydrometallurgical routes. This research is being conducted under the Minerals Down Under Flagship and is being used to identify opportunities for reducing impacts in greenhouse gas emissions, water consumption, resource depletion and waste generation, and to improve efficiency during mining, mineral processing and metal production.

A recent study estimated the expected life of various metals (Cohen, 2007). This study showed that this can be from four years for indium to 500 years for aluminium based on the current US per capita consumption rate. Some of the metals are scarce or abundant or in high demand but others are not so at this point. Some of the very useful metals are expected to be depleted within half the lifetime of a single human generation. For example, copper is a very useful metal for modern civilisation. The expected life in the worst case scenario is 38 years and the best case is about 76 years. This poses a serious challenge for human and industrial society for progress and development. However, the assumptions are based on no exploration and finding of new deposits, no technological efficiency enhancement, and also do not take into account variation in consumption rates. This study also emphasised prudency in utilising resources. Most of these metals' energy intensity, greenhouse gas footprint and water usage are reasonably high, and waste to product ratio is generally above 10. This is why it is very important to look at metal life cycles and to find where the main opportunities are to reduce significant environmental impacts.

In the last decade, LCA research work by CSIRO in the minerals domain focused on metal production including ferro-metal, other base-metal and also some light metals, covering both hydrometallurgical and pyro-metallurgical routes. Although greenhouse gas emissions from mining activities are generally low, a recent study was undertaken to look more closely at the LCA of iron ore, Cu and bauxite mining (Norgate and Haque, 2010). Currently, work is being undertaken on both mining and metal production of uranium, gold, nickel, manganese, and magnesium in further detail. There is a significant project to reduce the greenhouse gas impact of steel making using biomass char and its various aspects.

The main selected environmental impact categories are gross energy requirement (GER) which is used to estimate global warming potential (GWP) or greenhouse gas emissions in CO_2 equivalent units, solid waste burden, and water usage. Recently, toxicity impacts

of minor elements in some waste streams in the metal production chain have been included in the LCAs, as well as reviewing the methodology for including socio-economic impacts in LCAs. There are other impact categories but some are quite challenging to quantify and include in every case (for example, biodiversity and land-use).

Aluminium smelting is very much electricity-intensive. Use of SimaPro LCA software is convenient for this case since it contains an Australian database. In most cases, Australian electricity factor for greenhouse gas emission in the SimaPro Australian database has been changed to assess GWP impact. However, for those products and processes that are not as electricity-intensive as aluminium smelting, SimaPro database should be used carefully and further judgement should be applied on the results by the LCA practitioner.

Comparing the LCA results for various metals on a "cradle to gate" basis in terms of GHG emissions, showed that aluminium had the highest emissions per tonne of metal followed by nickel and copper (Figure 1). However, it is interesting to note that when these unit emissions are combined with the total production volumes of these metals, both in Australia and globally, steel was found to be more significant globally than aluminium because of the magnitude of its production compared with aluminium (Figure 2). Similarly, in mining activities, the impact of copper is greater because of the low ore grade, so a larger quantity of ore must be processed (Figure 3). Results of the steel LCA showed that the blast furnace is the main opportunity in terms of CO_2 reduction from the steel industry.

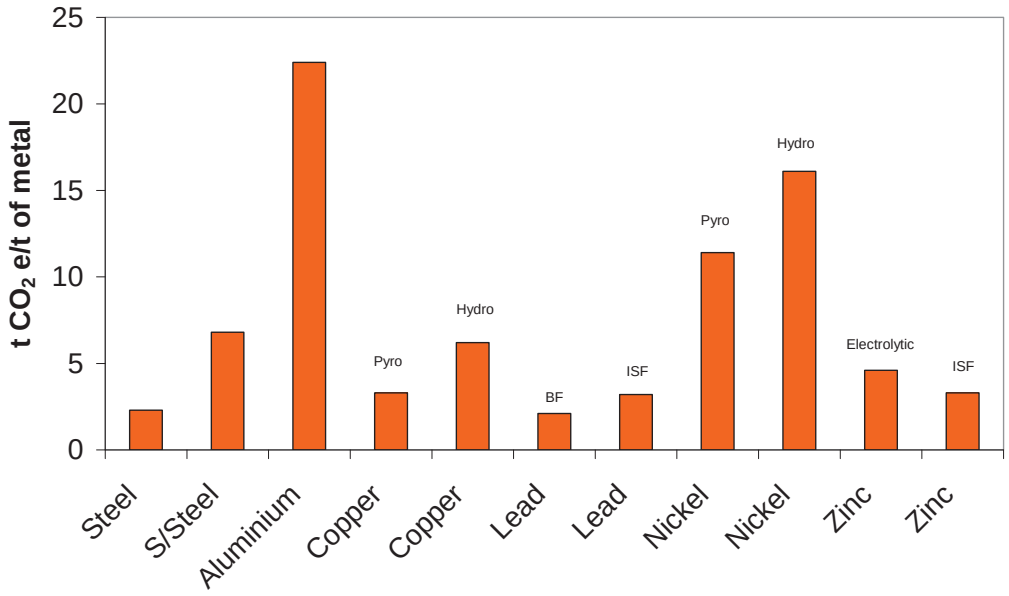

Figure 1: "Cradle to gate" LCA for various metals.

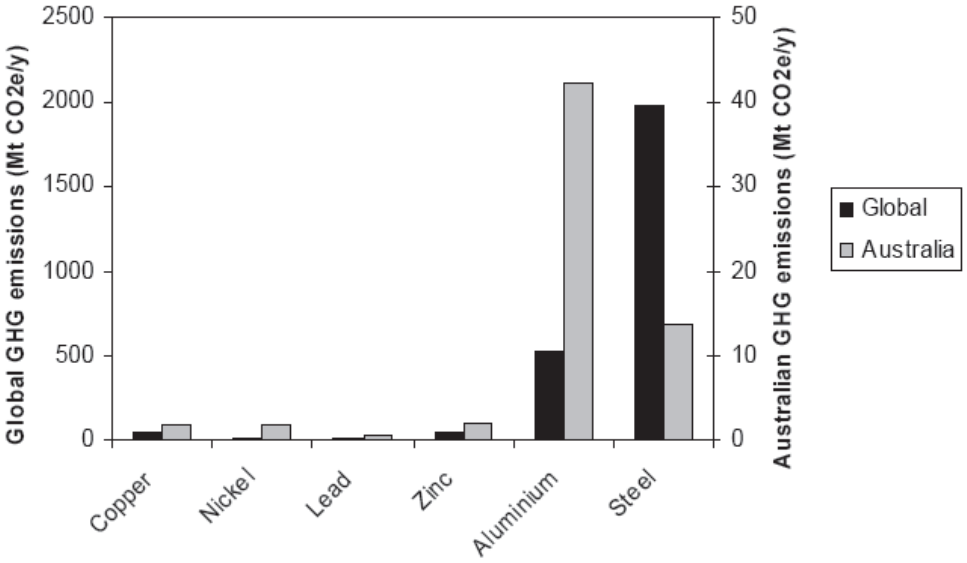

Figure 2: Overall GHG emission from various metals.

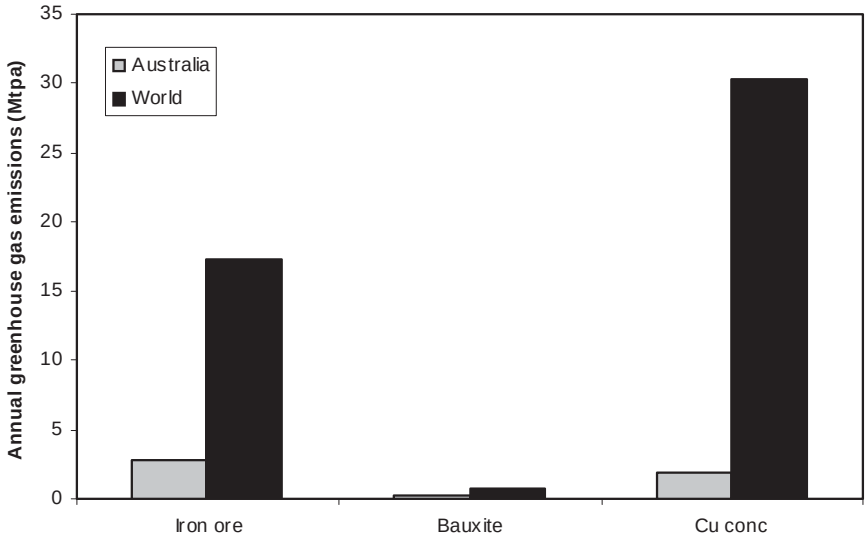

Figure 3: GHG emission from mining activities.

The conventional blast furnace route for steel production produces about two tonnes of CO_2/t of steel. Charcoal made from biomass can be applied in steel making to reduce these CO_2 emissions. Plantations can be raised to absorb CO_2 through photosynthesis. When mature trees are processed for sawn timber and other wood products, waste residue can be used for making charcoal for steel making.

In terms of water usage for metal production, the LCA studies have shown that apart from gold which is the most water-intensive (Figure 4), the water intensity of titanium is about five times that of copper (Norgate and Lovel, 2006).

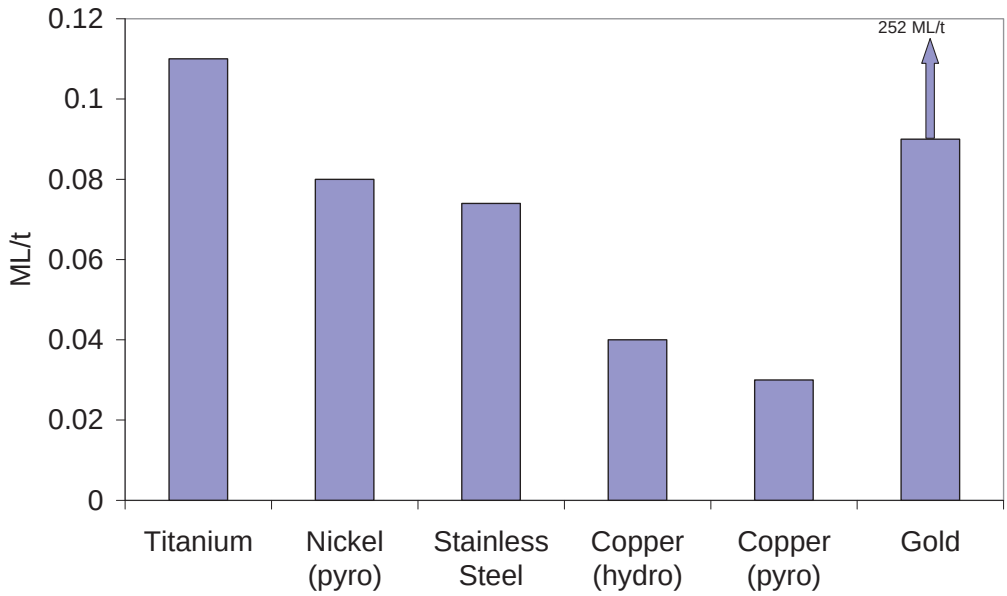

Figure 4: Water footprint of metal processing.

LCA methodology can be used to obtain a true environmental picture of a process over its entire life cycle, thereby identifying those parts of the metal production life cycle that have high environmental impacts. Reducing any increase in demand for primary metals in the future through dematerialisation, re-use and recycling will also help alleviate the environmental impacts associated with primary metal production.

References

[1] Cohen, D., Earth audit. *New Scientist* 195(2605):34-41, 2007.
[2] T. Norgate, N. Haque, Energy and greenhouse gas impacts of mining and mineral processing operations. *Journal of Cleaner Production,* **18**, 266-274, 2010.
[3] Norgate, T., R. Lovel, Sustainable water use in minerals and metal production. Proceedings of the Green Processing Conference, 5-6 June, Newcastle, Australia, 2006.
[4] T. Norgate, S. Jahanshahi, W.J. Rankin, Assessing the environmental impact of metal production processes. *Journal of Cleaner Production,* **15**, 838-848, 2007.

Corresponding author's email: Nawshad.Haque@csiro.au Tel: 03-9545 8931.
Web: www.csiro.au/people/Nawshad.Haque.html

SOME COMMENTS ON THE STUDY OF METALLURGICAL COKE AND ITS USE IN THE IRON BLAST FURNACE: UNDERSTANDING PROCESS FUNDAMENTALS THROUGH LABORATORY STUDIES

B.J. Monaghan[1], M.W. Chapman[1,2], S.A. Nightingale[1], J.G. Mathieson[2] and R.J. Nightingale[2]
[1]PYROmetallurgical Research Group, University of Wollongong, NSW 2522, Australia
[2]BlueScope Steel Limited, P. O. Box 202, Port Kembla, NSW 2505, Australia

Keywords: ironmaking, coke, coke analogue

Much of the recent experimental work carried out at by the PYROmetallurgical group at the University of Wollongong has focussed on understanding coke behaviour in the lower zone of the blast furnace. This work has had both fundamental and applied elements and has been carried out with a view to improving coke utilization in the blast furnace and ultimately reducing greenhouse gas emissions. Brief details of the some of this research are given below.

Mineral Layer Effects on Coke dissolution in Iron

An experimental study of the effect of a mineral layer formation on coke dissolution kinetics in liquid iron has been carried out. The system studied was designed to in part replicate the relatively quiescent conditions in the deadman area of a blast furnace. In this investigation a clear relation between the kinetics of coke dissolution and the morphology of the layer formed on the coke was established [1]. Experimental findings are shown below in Fig. 1 and Fig. 2 for the predominant phases at the coke-iron interface and first order rate plots respectively. The change of slope shown in Fig.2's first order rate plots represents a slowing of the rate of coke dissolution.

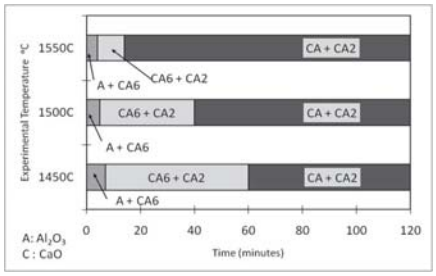

Fig.1. Predominant mineral matter phase(s) at the coke–metal interface verses experimental time.

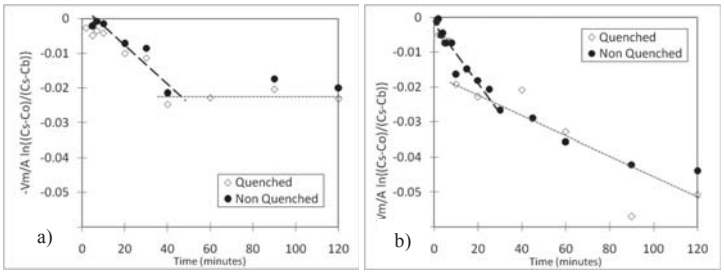

Fig. 2. First order mass transfer control plots for a) 1500°C and b) 1550°C.

Though not shown in Fig.2, similar results were found for coke dissolution at 1450°C. The change of slope is coincident with the appearance of the more dense CA ($CaO.Al_2O_3$) phase noted in Fig. 1. This finding is considered evidence of a reaction blocking mechanism slowing the dissolution kinetics, where the formation of a dense layer reduces the contact between the coke and liquid iron.

Deadman Coke Fines and Their Sources

There was some ambiguity as to the source of coke fines (generally less than 8mm but 1 to 4 mm in this study) found in deadman area of a blast furnace [2]. To identify the source of these coke fines tuyere probe samples were obtained from both the deadman and raceway areas of the blast furnace (see Fig.3 .) Using measurements of L_C, it was established that some of the fines found in the deadman area of a blast furnace were not simply the degradation products of the lump coke in this area. The coke fines had a higher L_C than the coke lump and therefore had experienced a higher temperature than the associated coke lump. Fig. 4 shows typical L_C measurements for the tuyere probe coke samples. This finding has been interpreted as indicating that at least some of the coke fines are being blown into the deadman area (lower temperature region) from the raceway by the high velocity hot blast.

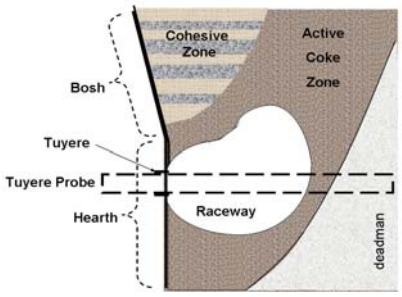

Fig.3. Schematic showing the tuyere probe and key zones in the lower zone of the blast furnace.

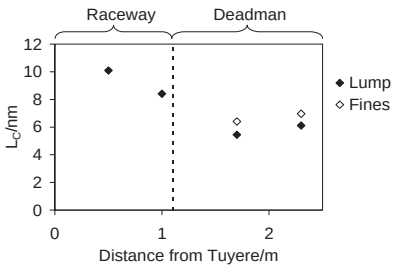

Fig.4. L_C measurements for the tuyere probe coke samples 12/02.

The Development of a Coke Analogue for the Study of Important Coke Reaction Phenomena

Industrial coke is not an ideal laboratory reagent. It has inherent heterogeneity problems with respect to oxide phase composition and phase dispersion not to mention coke porosity variability that often mask or complicate the coke reaction behaviour that is of interest in the metallurgical industries. To overcome this heterogeneity problem an idealised coke analogue material has been developed in which the mineral phase's composition, morphology and dispersion and the overall porosity can be controlled. Details of the analogue are given and its abilities to represent coke are assessed and discussed. It is envisaged that this coke analogue material will have much to offer in future studies of coke reaction behaviour, particularly in areas where mineralogy of the coke ash is considered to affect coke reactivity. There may also be coal applications of this analogue that are of interest to the power generation industries that have similar heterogeneity problems to coke when trying to understand coal reaction behaviour.

References

[1] M.W. Chapman, B.J. Monaghan, S.A. Nightingale, J.G. Mathieson, and R.J. Nightingale, Formation of a Mineral Layer During Coke Dissolution into Liquid Iron and its Influence on the Kinetics of Coke Dissolution Rate, *Metallurgical and Materials Transactions B*, **39B**, 418-430, 2008.

[2] B.J. Monaghan, R. Nightingale, V. Daly and E. Fitzpatrick, Determination of the Thermal Histories of Coke in a Blast Furnace Through X-ray Analysis, *Ironmaking and Steelmaking*, **35**, 38-42, 2008.

BLAST FURNACE IRONMAKING WITH LOW COKE CONSUMPTION

Guangqing Zhang
School of Materials Science and Engineering, the University of New South Wales,
UNSW SYDNEY, NSW 2052, Australia

Key words: Ironmaking, Blast Furnace, Reduction of Coke Consumption

Blast furnace (BF) ironmaking is the major process for iron production. It is a well-established and highly efficient process in terms of energy and exergy consumption [1]. However, BF ironmaking is a major source of CO_2 emission. BF ironmaking is based on the usage of coke as both reductant and fuel. Coke is expensive, and its production causes environmental concern. Further development of BF ironmaking targets decreasing coke consumption and overall CO_2 emission.

Over the last twenty years great efforts have been made to decrease coke consumption in the BF ironmaking using pulverised coal injection (PCI) [2,3]. In the best PCI practice, about 200 kg pulverised coal (PC) per tonne of hot metal (THM) has been injected in continuous operation, and 260 kg/THM for a short period [4]. However, further increase of the PCI is limited: the injected pulverised coal is only partly combusted in the raceway; the unburnt char is accumulated within a BF, especially in the cohesive zone, decreasing the gas permeability of the furnace and limiting the BF productivity [5,6].

Coke in the BF operation is consumed by direct reduction of FeO, combustion in raceway to provide heat for the BF operation and generate CO which is used as a reducing gas, dissolution in hot metal, and by reduction of nonferrous elements. The latter two items change in a relatively narrow range; they can be assumed to be unaffected by the BF operation. Modification of the BF to decrease the coke consumption targets the former two quantities which can change significantly depending on the practical operation, and theoretically can be reduced to zero. Under these conditions, the consumption of carbon from coke will be at a level of 53 kg/THM, or equivalent to about 70 kg/THM coke. This coke consumption is considered as a theoretical limit in operation of a BF, which is referred to in this paper as a new generation BF. Carbon needed for reduction of iron oxides and heat generation can be provided by injecting pulverised carbonaceous materials. Operation of this furnace is described below.

Complete combustion of injected pulverised carbonaceous materials. Carbonaceous materials are injected through the tuyeres without accumulation of char residue. Their combustion will totally satisfy furnace heat requirements; no coke will be combusted or gasified in the raceway.

Complete reduction of FeO in the solid state within the isothermal zone. Complete or near complete reduction of iron oxides in the solid state within isothermal zone will exclude consumption of coke by direct reduction.

In the conventional BF operation, the degree of metallisation by indirect reduction is 30-60%. A significant amount of FeO enters the cohesive zone causing softening of the burden and formation of the primary slag. When FeO is totally reduced in the solid state, the liquidus temperature of the FeO-free burden will be high and formation of primary slag will be avoided.

Metallic iron formed by reduction at low temperatures will contain relatively low carbon; it is expected that it will not melt below 1400 °C. As a result, in the new generation BF, molten iron and slag phase will form above 1400 °C. Due to very high temperature gradient in the section, relatively narrow temperature range of melting iron and slag, and low viscosities of the molten phases, the cohesive zone will be suppressed to a very thin layer, which will improve the permeability of the stack. This will allow operation of the BF with low coke rate.

CO recycling and N_2 free operation. To decrease emission of greenhouse gases by the steelmaking industry, ULCOS (Ultra-Low CO_2 Steelmaking program involving 47 partners in EU) is developing a nitrogen free BF and CO_2 capture and storage. The program considers injection of CO after CO_2 capture into the BF through the BF stack. Non-uniform gas distribution across the radial section of a BF stack is a serious problem in realisation of this program [5]. In the new generation BF operation, CO is injected both through the tuyeres and into the isothermal zone. The ratio between CO injected through the tuyeres and into the isothermal zone will be controlled by the theoretical flame temperature for the nitrogen-free BF operation.

Energy and exergy analyses were carried out to identify the potential of energy saving and reduction of carbon consumption in a new generation BF [7]. The base case is represented by a conventional BF with 200 kg PCI/THM. The top gas containing CO, CO_2 and N_2 is used to preheat the blast. Assuming a heat efficiency in a stove of 80% (exergy efficiency 47%), 398.3 kg/THM carbon is consumed, among which 198.3 kg/THM is from coke.

The operation of a new generation blast furnace is assumed with a complete recycling of the CO separated from the top gas which is injected through the tuyeres and into the isothermal zone. The fraction of CO injected through the tuyeres and into the isothermal zone is adjusted to control the theoretical flame temperature at 2400 °C. Under these conditions, the overall carbon consumption is decreased to 378.5 kg/THM. At the same time, the bosh gas flow is decreased by 43.6% relative to base case. The net energy consumption is by 4.8% higher than in the conventional blast furnace. This slightly higher energy consumption can be compensated easily by preheating the cold blast oxygen and recycled CO using the low temperature waste heat such as the top gas before wet-scrubbing.

In conclusions, successful operation of a new generation BF with low coke consumption is based on complete combustion of injected carbonaceous materials, nitrogen-free blast, recycling of CO of the top gas, and 100% indirect reduction of wustite. The coke consumption in the BF can be reduced to a level below 100 kg/THM. The proposed new generation BF has a higher exergy efficiency and lower carbon consumption, but the net energy consumption is marginally higher than in the conventional BF. Preheating of the CO injected through the tuyeres using a low temperature heat source further increases the efficiency of BF operation.

References

[1] Biswas A. Principles of Blast Furnace Ironmaking. Cootha Publishing House, Brisbane, 1981.

[2] IEA Clean Coal Centre Report: Use of PCI in Blast Furnaces. October 2006.

[3] Office of Industrial Technologies, Energy Efficiency and Renewable Energy, U.S. Department of Energy: Pulverised Coal Injection (PCI) Coal Combustion Behavior and Residual Coal Char Carryover in the Blast Furnace during PCI at High Rates. January 2002.

[4] Decker A. and Poos A. Stahl u. Eisen, 1972, 92, 1077-1084.

[5] Buchwalder J., et al. Development of Injection of Reduction Gas into the Blast Furnace Shaft, In: Metec InSteelCon, 2007, Dusseldorf, 298-305.

[6] Ohno Y. et al. Process Characteristics of a Commercial-scale Oxygen Blast Furnace Process with Shaft Gas Injection. ISIJ Int., 1992, 32(7), 838-847.

[7] Zhang G. and Ostrovski O. Energy and Exergy Analyses of Low Coke Blast Furnace Ironmaking. In: Proc. 5th Intern. Con. Sci. Technol. Ironmak. 603-607.

LARGE SCALE COPPER SMELTING USING AUSMELT TSL TECHNOLOGY AT THE TONGLING JINCHANG SMELTER

Jacob Wood
Ausmelt Limited

From an established base for treating a range of non ferrous metals, Ausmelt Top Submerged Lance (TSL) Technology has demonstrated its ability to adapt to new applications and the processing of different feed types. In the copper industry alone, the technology spans a range of processes from primary smelting through Continuous Copper Converting (C3) and the treatment of secondary copper feeds to address the emerging metals recycling market. Additionally, the ability to scale plant operation and to address industry driven demands of improved environmental performance along with increased capacity and flexibility makes Ausmelt TSL a pivotal copper production technology into the future.

This paper examines the large-scale implementation of Ausmelt Technology for the smelting of copper concentrates at the Tongling Jinchang Smelter and how this plant rapidly achieved its design rate of 65,000 tpa copper production and has subsequently been expanded to now produce over 175,000 tpa copper.

DISTRIBUTION OF BISMUTH BETWEEN COPPER AND FeO_X-CaO-SiO_2 SLAGS AT 1300^{O}C

Lidya Paulina, Prof. Doug Swinbourne
RMIT University

The Peirce-Smith converter, using iron silicate slag, has been used in industry for over a century for copper matte converting. However, the increasing cost of energy and stricter environmental regulations have led to the development of more efficient continuous copper converting processes. Choice of slag composition is important in copper converting. Iron silicate (FeO_x-SiO_2) slag attacks magnesia-chrome refractories to a very limited extent and has a high capacity for absorbing basic oxides such as lead oxide. Unfortunately, during converting, where the oxygen partial pressure is high, magnetite solubility becomes low. This results in a viscous slag which decreases the slag tapping rate and increases the extent of copper entrainment in slag. Calcium ferrite (FeO_x-CaO) slag was pioneered by Mitsubishi for their continuous converting process and offers benefits including low viscosity, high magnetite solubility and a high capacity to absorb acidic oxides such as those of antimony and arsenic. It has the disadvantage of very aggressive attack of magnesia-chrome refractories. Ferrous calcium silicate – FCS - slag (FeO_x-SiO_2-CaO) has been proposed as a third slag for copper converting. It has been shown that FCS slags attack refractories much less than calcium ferrite slag, however little is known about the distribution ratio of minor elements between FCS slags and copper.

One minor element of interest is bismuth. Bismuth has long been known to adversely affect the mechanical properties of copper. It can be removed during copper electrorefining but excessive amounts of impurities in anode copper leads to an increase in expensive bleed stream treatment. The amount of impurities in anode copper therefore needs to be minimised. Surprisingly, the distribution behaviour of bismuth during copper converting has been little studied. In this project the distribution of bismuth between molten copper and slag will be mapped over all slag compositions which are liquid in the copper-saturated FeO_x-SiO_2-CaO system at 1300 ^{o}C and an oxygen partial pressure of 10^{-6} atm.

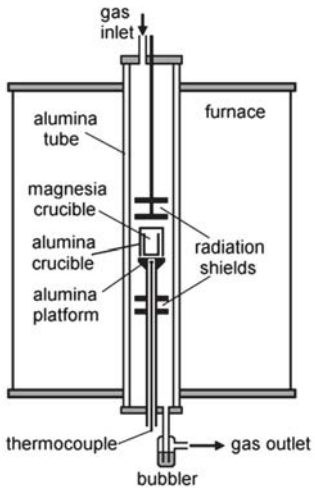

The experimental method used is the classical three-phase equilibration technique and the apparatus used is shown in the adjacent figure. Slags of various compositions, defined by their CaO contents and Fe/SiO_2 ratios, are contained in a magnesia crucible together with copper. An inverted alumina crucible is used to minimise the loss of bismuth through volatilisation. The oxygen partial pressure is determined by the flow rates of carbon monoxide, carbon dioxide and nitrogen – which are set by mass flow controllers. A dibutylphthalate bubble is required to prevent back-diffusion of oxygen from the air. It is essential to be certain that chemical equilibrium has been achieved so two sets of experiments are performed for each slag composition. In one set bismuth is initially added to the

copper, and in the other set $BiO_{1.5}$ is added to the slag. After the predetermined time of contact the crucible assembly is lowered into the cool zone of the furnace and then removed. The copper and slag are separated and carefully cleaned, then analysed for bismuth and, in the case of the slag, CaO, SiO_2, MgO, Cu and total iron contents.

The distribution data is presented in the form of a ratio (L_{Bi}) of the bismuth content of the slag divided by that in the copper. The system can be assumed to have reached equilibrium when the same ratio is reached, independent of contact time and of the direction the equilibrium was approached. The results for one slag are given in the adjacent figure. It can be seen that, within experimental error, the same value of distribution ratio has been achieved for all data points, so the average value is taken to be the true value. It is also apparent that under copper converting conditions bismuth distributes preferentially to the copper metal. This, unfortunately, is detrimental for the effective removal of bismuth from anode copper.

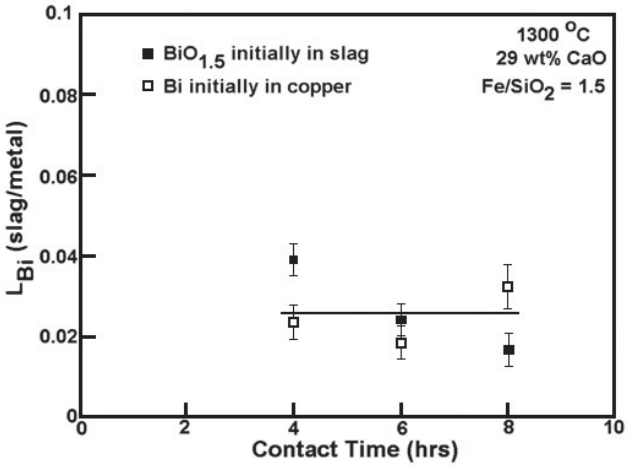

Minor element distribution behaviour is also affected by the composition of the slag, but to varying extents depending on the nature of the minor element oxide. If, for example, it is acidic in character then the minor element will partition more to slags that have low acidic oxide (SiO_2) contents and high basic oxide (CaO) contents and thus the value of L_{Bi}(slag/metal) will increase. The final figure shows the liquid region of slags in the copper-saturated $CaO\text{-}SiO_2\text{-}FeO_x$ system, presented in a form developed by Kongoli and Yazawa. Only five slag compositions have been examined to date. Within experimental errors, it appears that the bismuth distribution ratio is not much affected by slag composition. Changing slag composition to better control bismuth in anode copper seems not to be an option available to the smelter. However, much more work needs to be done to confirm this early conclusion and to map the actual bismuth distribution ratio over the liquid region.

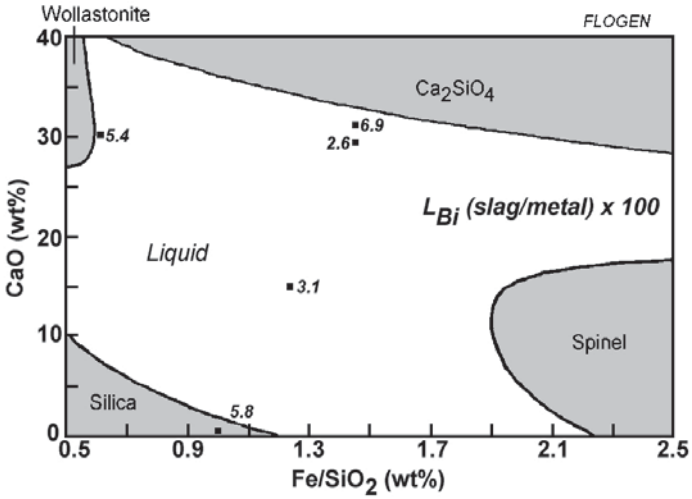

PHYSICAL MODEL STUDIES OF SOME METALLURGICAL PROCESSES

John J.J. Chen
Chemical and Materials Engineering Department
The University of Auckland, Private Bag 92019, Auckland 1142, New Zealand
Tel: +64-9-9238137, Fax: +64-9-3737463, E-mail:j.chen@auckland.ac.nz

Many metallurgical processes are conducted at high temperatures and they normally operate in a very corrosive and hostile environment. Many important design, control and operating parameters may not be obtainable directly from the actual high temperature processes. High temperature bench-scale studies have been conducted to provide some information for certain aspects of the processes but the influence of scale is often an issue. Computer modelling has also provided very useful insights, and aids in the design of equipment, the operation, control and optimisation of the processes. Room temperature physical analogue model studies are able to provide further detailed understandings, and generate data for the validation of the computer models. In this presentation, some room temperature physical analogue model studies of the aluminium smelting process, the treatment of molten aluminium, the flow and temperature fields in a direct-reduction iron-making melter, and the flow of molten steel in a tundish will be presented. The following figures show some of the equipment used.

Figure 1. A full-scale aluminium smelting cell model used for the study of bubble-induced fluid circulation and mixing, side wall heat transfer, etc.

Figure 2. Full-scale model of a molten aluminium treatment furnace for the study of mixing, flow pattern and bubble dispersion.

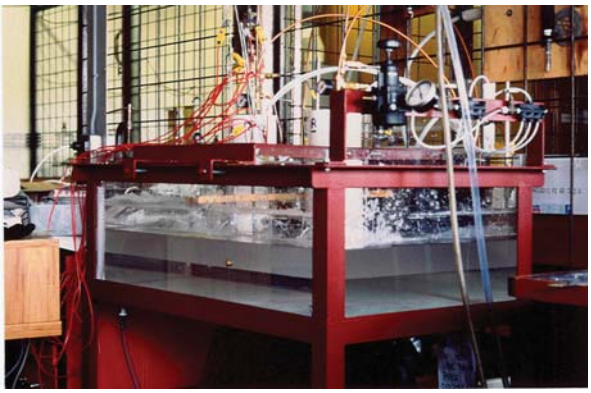

Figure 3. A scaled model of a direct reduction iron-making melter using wax to represent the slag, water the iron, and air the carbon dioxide formed, for the study of temperature distribution, flow distribution and mixing.

Figure 4. A One-third scale model of a tundish for the study of steel flow, mixing and residence time distribution.

ONLINE ANALYSIS OF BUBBLE FLOW IN METALLURGICAL OPERATIONS

Xiaodong Xu[1], Geoffrey Brooks[1] and William Yang[2]
[1]Faculty of Engineering and Industrial Science
Swinburne University of Technology
Hawthorn, VIC 3122, Australia

[2]CSIRO Minerals
Box 312, Clayton South, VIC 3169, Australia

Keywords: Ladle metallurgy, Process control, Pyrometallurgy, Bubbling phenomena, Online sensors, Principal component analysis (PCA)

Bubbling is commonly used in pyrometallurgical vessels to enhance mass and heat transfer. These processes can be difficult to monitor because of the severe operating conditions associated with these processes. Cold modeling experiments have been performed to analyze all the signals of the bubble flow inside a cylindrical vessel, which is shown in Fig 1[1]. The inner diameter and height of the vessel are 420 mm and 500 mm respectively, representing a $1/10^{th}$ scale steel ladle. The height of water was kept 210 mm to simulate liquid steel; and the depth of motor oil (SAE 20,density $\rho=0.85\times10^{-3}kg/m^3$) which simulated slag, varied from 5 mm to 20 mm in 5 mm increments. The color of the oil was light brown and could be easily discriminated from the water by the naked eye. Compressed air was injected into the bath through a 3-mm nozzle flush at the bottom of the vessel at flow rate varied from 2.0 to 20.0 lpm at 2.0 lpm intervals. The air pressure was fixed to 200.0kPa at the exit of a compressed gas tank and the air flow rate was controlled by a standard rotameter with an accuracy of 3%. A digital video camera was used to record images (960×720 pixels) at 15 frames per second, and an accelerometer was installed on the outside wall of the vessel to collect the vibration signals.

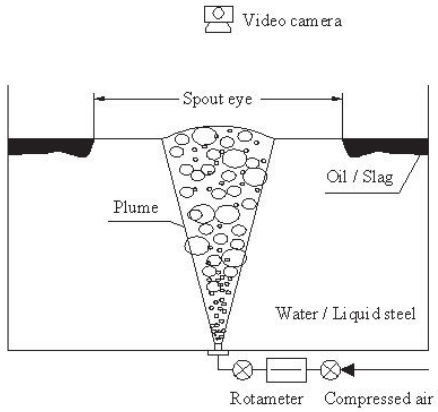

Figure 1 - Schematic diagram of the cold modelling apparatus[1]

It is clear that the size of the spout eye area, the sound of the bubbling and the vibration on the wall of the vessel are all generated from the same stirring and they should be correlated. Though there are several techniques available to investigate multivariate data

sets, such as neural networks and fuzzy logic, Principal Component Analysis (PCA) approach was applied because it is easy to operate and have been proved to be very powerful in reducing the dimension of variables, and also because it is suitable for online analysis which is particularly important for online control. Image and sound signals were separated from the video stream by commercial soft wares and all the three signals were organized into a state matrix after they were pre-treated individually. The strategy to analyze the signals is shown schematically in Fig 2.

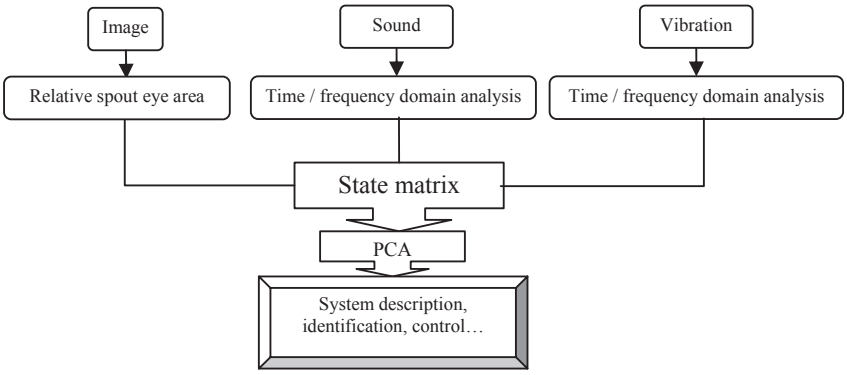

Figure 2 - Schematic diagram of signal analysis strategy used in this study

The spout eye area was calculated by a threshold technique [2] and was turned into relative spout eye area which is the ratio of the area of spout eye and the intersection of the vessel. The sound and vibration were measured by both intensity and spectrum.

The results demonstrated that the image signals of the disturbed top surface, sound of bubbling and the vibration on the wall of the vessel are highly correlated, and they can be reduced to just one signal which captures most of the variations of the bubbling phenomena. This signal can be expressed by the linear combination of the five variables, and it has a clear linear relationship with stirring power, which can be used to indicate the stirring process. It also statistically proved that the combined signals from sound and vibration can catch up most of the variation of the stirring process, and they can be measured in either time domain or frequency domain. This combined signal can be used as a feed back signal for the process control and may lead to the development of online sensors. The image signal provides trivial contributions to the total variation of the process, and the process can be monitored without it. This finding is particularly important for the pyrometallurgical operations in which it is difficult to install a digital camera above the vessel.

References

1 K. Krishnapisharody and G. Irons, *Metallurgical and Materials Transactions B* **37**, 763-772 (2006).

2 X. Xu, G. A. Brooks, W. Yang and C. Stefanie, *Ironmaking and Steelmaking: Processes, Products and Applications*, Accepted on 03/11/2009 (2010).

FACTORS AFFECTING NICKEL EXTRACTION FROM THE REDUCTION ROASTING OF SAPROLITE ORE IN THE CARON PROCESS

J. Chen, E. Jak, P.C. Hayes

Pyrometallurgy Research Centre
School of Engineering, The University of Queensland
Brisbane, QLD 4072, Australia

Keywords: Saprolite, Reduction Roasting, TEM

Laboratory investigations have been undertaken to simulate conditions occurring during the reduction roast step of the Caron Process to obtain improved understanding of the factors influencing nickel extraction from Saprolitic ores. Saprolite samples have been treated at temperatures between 500^{o}C to 800^{o}C in H_2/N_2 gas mixtures, and leaching tests on reduced samples have been undertaken.

Phase and microstructure changes have been characterised using X-ray powder Diffraction (XRD), Scanning Electron Microscope (SEM) and Transmission Electron Microscope (TEM). A phase transformation from Lizardite to X-ray amorphous material and eventually to olivine has been observed associated with evolution of porous structure. Reduced Ni has been found in the form of Ni-Fe alloy nanoparticles with size less than 20nm.

Ni recovery from reduction roasted Saprolite after ammonical leaching increases with increase of reduction temperature, and reaches to maximum at 700^{o}C-750^{o}C, significant drop of Ni recovery is found when reduction temperature is higher than 750^{o}C. At reduction temperature range from 500^{o}C to 650^{o}C, Ni recovery increases with increase of reduction time, however, long reduction time in the temperature range from 700^{o}C-800^{o}C has negative effect on the Ni recovery.

A reaction scheme may be proposed for reduction roasting of Saprolite.

- Dehydration takes place, chemically bonded water is removed and creating a porous structure
- Reduction takes place at Ni-Fe enriched areas and Ni-Fe alloy nano-precipitates form
- Re-crystallization of olivine takes place; fine pores coarsen and close up to reduce the surface energy. Some previously formed Ni-Fe alloy nano-precipitates are physically trapped in the closed pores and become inaccessible to leaching liquor, reducing nickel recovery overall

DEVELOPMENT OF A HIGH FLUX SOLAR FURNACE FACILITY AT CSIRO FOR HIGH TEMPERATURE PROCESSES

James T. Hinkley[1], Robbie K. McNaughton[1]
[1]CSIRO Energy Technology

Keywords: Solar furnace, concentrated radiation, flux, smelting, materials evaluation.

CSIRO is currently developing a concept proposal for the construction of a high flux solar furnace in Australia. The proposal meets the needs of both research and industry by providing critical infrastructure to enable development of technologies to exploit Australia's high quality solar resource. The furnace would be hosted by CSIRO at the National Solar Energy Centre in Newcastle, and could be available for the first experiments within two years from project approval. The design of the facility will be developed in consultation with Australian and international experts to ensure that it is both state-of-the-art and relevant to the needs of local researchers and industries. There are only a handful of such facilities world wide and none in the southern hemisphere.

Solar furnaces are advanced thermal facilities which can achieve very high solar concentrations of more than 5000 times that of the sun ("5000 suns"), resulting in surface temperatures over 2700 K. The proposed furnace will be designed to deliver between 25 and 50 kW at peak fluxes of over 4000 kW/m².

These high fluxes are achieved using a flat heliostat to track the sun and direct the radiation onto extremely precise concentrating facets which focus the energy into a spot as small as 15 cm in diameter. The proposed facility would employ an "off-axis" design, meaning that the focal point is offset from the line between the heliostat and the concentrator. This enables far more sophisticated and precise control of the experimental conditions, as the focal point can be located in an experimental chamber in a dedicated building. The Australian High Flux Solar Furnace will be the most advanced solar furnace to be constructed, building on overseas experience in constructing and operating such facilities. The solar furnace will provide a cost effective and realistic platform for experiments, which can be much more easily set up at ground level. This greatly simplifies access, reticulation, control and monitoring compared to small experiments conducted using a heliostat field and tower or dish system.

This facility would provide the necessary infrastructure to enable the assessment of high temperature materials and processes to put Australia at the forefront of high temperature thermal research. Potential applications of the solar furnace include the following:

- **Evaluation of concentrated solar energy for minerals and metals processing.** Australia has tremendous resources of both solar energy and mineral wealth, and these are often co-located. Fundamental and applied research is required to understand the heat and mass transfer considerations around solarising of roasting and smelting of minerals and metals.
- **Evaluation of materials and components for higher temperature solar thermal power generation.** One of the most promising avenues for reducing

the cost of solar thermal electricity is improving the conversion of solar energy to electricity by operating at higher temperatures and using more thermodynamically efficient cycles. However, operating at higher temperatures requires dealing with more concentrated solar radiation with increased risk of "hot spots" and elevated thermal stresses due to higher heating rates. Materials of construction for high temperature solar receivers pose a significant challenge requiring realistic assessment under comparable conditions to real world applications, as it is the interaction of concentrated radiation with the material that is of interest rather than purely the temperature achieved.

- **Thermochemical processes for storage of solar energy in fuels.** A key challenge of solar energy is its inherent intermittent nature. Storing solar energy in chemical bonds offers the ability to embed this energy in a transportable form for exploitation as needed. Examples include the solar thermal reforming of methane to produce a higher energy syngas than the feed material, and thermochemical water splitting cycles for the production of hydrogen.
- **High temperature heat transfer fluids and thermal energy storage.** Solar energy can also be stored as sensible heat in high temperature fluids such as molten salts (traditionally potassium and sodium nitrate). Further research is needed in this area to identify stable materials with a higher upper operating temperature to increase storage capacity and allow interfacing with higher temperature processes.
- **High temperature and specialty materials development.** The ability to reach and maintain extreme temperatures enables the ready assessment and development of advanced ceramic and other materials for high temperature processes such as those found in combustion, gasification or pyrometallurgy.
- **Accelerated life testing and exposure to extreme radiation.** The solar furnace allows the evaluation of material stability under higher concentrations of radiation – this can range from accelerated life testing of specialty paints and coatings to extreme doses of high concentration radiation which simulate military and aerospace applications.

The Australian High Flux Solar Furnace will be an invaluable piece of advanced, enabling infrastructure that will allow Australian companies and researchers to be world leaders in the next generation of high temperature solar and thermal technologies. The facility will also provide a unique capacity for high temperature materials development with potential application to many industries including metal production and ore smelting. CSIRO welcomes any offers of participation in the development of this exciting project.

APPLICATION OF CURRENT-PULSE TECHNIQUES TO ANALYSIS OF ANODE GAS FILM BEHAVIOUR IN A HALL-HÉROULT CELL

Graeme Snook, Kathie McGregor, Andrew Urban and Marshall Lanyon
CSIRO Process Science and Engineering / Light Metals Flagship
Box 312, Clayton South, VIC, Australia, 3169

Keywords: electrowinning, aluminium, pulsed current techniques, capacitance, equivalent series resistance, bubbles

There is increasing pressure on aluminium smelters to reduce energy consumption in Hall-Héroult cells, for both cost and environmental considerations. A component of the cell voltage that is not well understood is the bubble–induced voltage drop at the anode, which has been estimated to be ~0.25 V [1]. It is very difficult to measure the bubble resistance in an aluminium reduction cell — a variety of approaches have been attempted, with mixed success [2].

In earlier work, CSIRO developed an *in-situ* galvanostatic technique that measures uncompensated resistance simultaneously with constant current or constant voltage operating conditions, to give the dynamic ohmic resistance [3]. One of the advantages of this method is that continuous measurements can be obtained during electrowinning, even in the presence of vigorous gas evolution. The purpose-built instrument, known as a 'resistometer', works in conjunction with a potentiostat and applies a square, bipolar current pulse (typically 1A) over a small timescale (~210μs) every 60ms to measure the resistance. As the pulse is bipolar, there is no net passage of charge, i.e., it is a rapid, bipolar and infrequently interrupted signal that does not significantly affect the Faradaic reactions or double layer charging. The device works on the principle that a current pulse will cause a corresponding voltage pulse according to Ohm's Law:

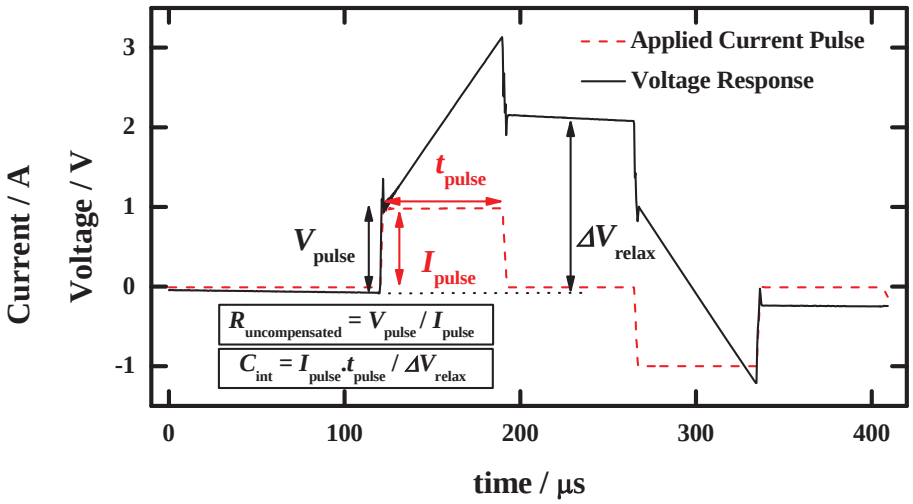

Figure 1 - Applied current pulse and corresponding voltage response with illustration of the in-situ measurement of resistance and capacitance.

$$V_{pulse} = I_{pulse} R_{uncompensated} \quad \textbf{(1)}$$

where V_{pulse} is the jump in voltage after application of the current pulse (I_{pulse}), from which the uncompensated (ohmic) resistance ($R_{uncompensated}$) can be calculated (see Figure 1).

The resistometer measurement can also be easily adapted to give the cell capacitance [4,5]. The capacitance is measured as:

$$C_{int} = I_{input} / (\Delta V_{relax} / t_{pulse}) \text{ or } C_{int} = I_{input}\, t_{pulse} / \Delta V_{relax} \quad \textbf{(2)}$$

where C_{int} is the capacitance, I_{input} is the current pulse magnitude (1 A), t_{pulse} is the time of the forward pulse (70 μs) and ΔV_{relax} is the voltage change from before the application of the pulse to during the rest period of the pulse (see Figure 1).

The capacitance values obtained from the current pulse method described here will depend on the sum of the capacitances active in the frequency range (~2–14 kHz), including those due to the double layer, impurity adsorption, charge transfer, corrosion etc. The values are not a true double layer capacitance, but allow changes in the electrode active area exposed to the molten bath to be measured. It is well-known that electrode capacitance is directly proportional to the surface area of the electrode [6], viz:

$$C = \varepsilon A / L \quad \textbf{(3)}$$

where ε is the permittivity, A is the area and L is the equivalent spacing of the capacitor plates (i.e., the double layer thickness). For the laboratory-scale aluminium reduction cell used in the anode effect studies, the cell capacitance is dominated by the carbon anode (the capacitance due to the cathode surface area is assumed to change very little) and the capacitance should give an assessment of the changes in anode surface area. A strong contributing influence to the capacitance will be due to anode bubble coverage (decreased surface area), but there may also be some effect from pitting and changes in the anode surface area as it is consumed.

In certain situations, using Ohm's Law to calculate the resistance measured by the resistometer gives an appreciable overestimation. Previously, we have modelled the electrode response from the resistometer using a Randles Equivalent Circuit (Figure 1), and found that if the cell interfacial capacitance is low (e.g., 30 μF), the shape of the voltage output pulse deviates markedly from that of the input current pulse (as in Figure 1) [7]. This indicates that the response is complex and not merely that of a simple resistor (i.e., there is a significant time-varying component). The overestimation can be overcome by applying a Fast Fourier Transform to both the input and output signals from the resistometer, and generating an electrochemical impedance plot from the current pulse data. Once the data is in the frequency domain, the time-varying component of the resistance is removed, leaving the equivalent series resistance (ESR) or solution resistance as the only residual resistance component (see Figure 2). The technique has been validated over a range of capacitance and resistance values using a Randles Equivalent Circuit, and a detailed description of the methodology is given in reference 7. The contribution of bubble evolution to the cell ohmic resistance can be calculated from the difference between the values measured at open circuit and during electrolysis. We have conducted a number of electrolysis experiments using our laboratory-scale aluminium reduction cell (see Figure 3), and found that use of the FFT

current pulse method was required to obtain an accurate assessment of the ohmic bubble resistance [8].

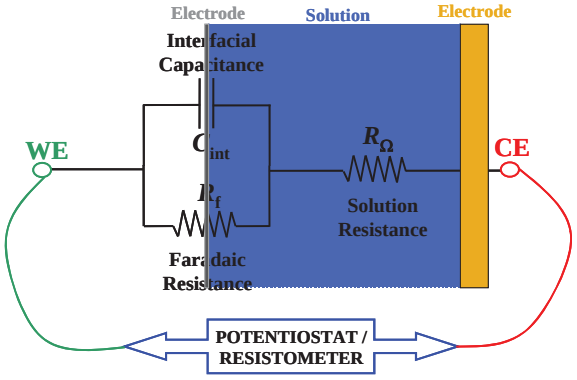

Figure 2 - Randles Equivalent Circuit, where R_Ω is the equivalent series resistance (ESR) or solution resistance, R_f is the Faradaic resistance, and C_{int} is the interfacial capacitance.

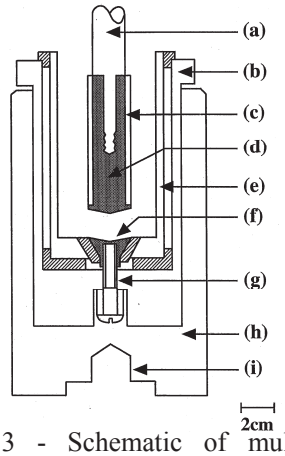

Figure 3 - Schematic of multi-element graphite cell [9]: (a) Inconel rotor shaft; (b) outer graphite sheath; (c) recrystallised alumina sheath; (d) graphite anode; (e) inner graphite sheath; (f) molybdenum cathode; (g) retaining screw; (h) graphite support shell; (i) rotator mount (hatched areas = boron nitride).

Application of these techniques to the lab-scale Hall-Heroult cell to measure changes in capacitance and resistance during aluminium production will be reported. Previously some preliminary measurements have been obtained [8] using standard and modified cryolite (lower temperature) compositions. In this paper, an extension of this work to a greater range of modified cryolite compositions is carried out. Upon application of the current ramp to the cell, the Equivalent Series Resistance (ESR) increased due to the bubble layer formed on the anode surface. Trends in ESR are examined in relation to the temperature and composition of the bath. The cell capacitance decreased due to the reduction of the available electrode surface area (now covered with bubbles). Estimates were made of the bubble coverage of the anode surface, and the trends supported the interpretation of data obtained from ESR measurements of bubble evolution.

References

[1] W. Haupin and H. Kvande, Light Metals, 379-384, 2000
[2] M.A. Cooksey, M.P. Taylor, J.J. Chen, JOM **60,** 51-57, 2008
[3] R.L. Deutscher, S. Fletcher , J.A. Hamilton, Electrochim. Acta, **31**, 585, 1986
[4] G.A. Snook, A.J. Urban, M.R, Lanyon, K. McGregor, J. Electroanal. Chem. **622**, 225, 2008
[5] G.A. Snook, K. McGregor, A.J. Urban, M.R. Lanyon, J. Solid State Electochem. **13** 591, 2009
[6] K.B. Oldham and J.C. Myland, *Fundamentals of Electrochemical Science*, Academic Press Inc., New York, 1994.
[7] G.A. Snook, K. McGregor, A.J. Urban, M.A. Cooksey, Electrochim Acta **54**, 2925, 2009.
[8] K. McGregor, G.A. Snook, N.V.Y. Scarlett, A.J. Urban, M.R. Lanyon, I.C. Madsen. "In-situ Analysis Methods for Electrowinning in Chloride and Fluoride Baths" Light Metals, 435-441, 2009.
[9] A.M. Vecchio-Sadus, R. Dorin, E.J. Frazer, "Evaluation of Low–temperature Electrolytes for Aluminium Smelting" J. Appl. Electrochem. **25**, 1098-1104, 1995 and references therein.

SIDEWALL MATERIALS FOR HALL-HÉROULT PROCESS

Reiza Mukhlis, M. Akbar Rhamdhani, Geoffrey Brooks
Swinburne University of Technology, Hawthorn, VIC 3122, Australia
Keywords: Aluminium, Sidewall, Hall-Héroult

ABSTRACT

The performance of current sidewalls made of carbon and silicon based materials relies on the existence of a frozen electrolyte layer. The development of the Hall-Héroult cell technologies such as inert anodes and wettable cathodes, call for new sidewall materials since the frozen ledge may no longer be applicable. Nickel ferrite has been identified as a possible sidewall material, particularly in relation to its resistance to cryolite and air attack. The presentation proposes some strategies to tackle the combined corrosive action of cryolite, molten aluminium and oxygen upon sidewalls. A multi-layer approach is proposed that optimizes both the chemical and heat flux requirements of a sidewall. Issues relating to joining of materials, process control, manufacturing, maintenance and cost need to be addressed before new sidewall designs can be implemented.

INTRODUCTION

The Hall-Héroult process is the only industrially viable method used to produce aluminium. The process is based on electrolysis of high purity alumina, which is dissolved into molten cryolite, and reduced to aluminium at 965 °C using carbon anodes. The overall chemical reaction in the carbon anode cell is as follows:

$$2Al_2O_3\,(dis) + 3C\,(s) = 4Al\,(l) + 3CO_2\,(g)$$

Recently, the process consumes about 13 kWh of electric energy to produce 1 kg of aluminium at a current efficiency of 100% [1]. It is estimated that more than half of the total energy requirement is lost as low grade heat, in which almost 35 % of the total heat loss is transferred through sidewalls [2].

The heat needs to be dissipated through the sidewalls in order to form a frozen layer of electrolyte to protect the sidewall materials from the attack of cryolite [3]. The heat dissipation to the side is also needed to prevent excess heat going up through the anode which can increase the chance of anode air-burning [4].

With the application of inert anodes, which is intended to reduce the greenhouse gas emission and process disturbances due to anode changing, the energy needed to produce aluminium is increased due to the absence of the carbon-oxygen reaction that provides energy [3]. The overall reaction would be:

$$2Al_2O_3\,(diss) = 4Al\,(l) + 3O_2\,(g)$$

In combination with wettable cathode or drained cell technology, it is possible to implement inert anode with the same energy consumption as carbon anode or even further reduce it by reducing the inter electrode distance [5]. However, the amount of heat needed to dissipate is also reduced, which make it difficult to form the electrolyte frozen layer [6].

In this case, the protective frozen ledge will be difficult to maintain and the sidewall materials will be exposed directly to the cryolite bath, which is likely to cause significant reduction on the life of the sidewall based on the current materials and design.

This condition calls for new sidewall materials that have high resistance against corrosion in the range of environments that exist within the cell. The materials should also have high thermal insulation, opposed to the current required sidewall material properties, in order to keep the heat inside the cell and maintain the heat balance of the cell.

Since the sidewall materials likely to be exposed to three different environments, namely reducing gas zone, corrosive bath zone and reducing molten aluminium, it would be difficult to develop a single material that can satisfy all required properties of the ideal sidewall materials.

NICKEL FERRITE AS SIDEWALL MATERIAL ALTERNATIVE

The desirable properties of sidewall materials are quite similar to that proposed for inert anodes and therefore, some of the inert anodes materials can be proposed as sidewall materials [7]. Both inert anode and sidewall material candidates should have low solubility in cryolite and aluminium; low porosity, not wetted by bath or metal, and high oxidation resistance. They also have to be mechanically robust to survive plant conditions, thermally stable, have adequate thermal shock resistance, and be easy to fabricate and join. The only significant difference on the required properties of sidewall materials and inert anode materials is on their electrical resistivity. With a modification in that property, i.e. doping, we proposed that inert anodes material may also be suitable as part of a sidewall design.

Among inert anode materials, nickel ferrite ($NiFe_2O_4$) based materials are of interest as sidewall material [7]. It has high thermodynamic stability [8] and corrosion resistance toward cryolite and alumina bath [9]. Study by Yan et al. [9] showed that the extent of corrosion of the nickel ferrite could be lowered by using high alumina content, close to alumina saturation. Yan et al. suggested that the corrosion of nickel ferrite due to dissolution in bath could be lowered by using low bath ratio. Their study showed that the solubility of the nickel ferrite was reduced when lowering bath ratio from 1.43 to 1.38. Laboratory test conducted by Olsen and Thonstad [10] on the nickel ferrite material showed that a dense oxide layer formed on the outer surface and it protects the material from further oxidation.

Hall-Héroult electrolysis cell can be divided into three different zones, namely the gas zone, the electrolyte (bath) zone, and the aluminium (metal) zone [11]. Each zone contains different chemical species and therefore has different characteristic. In the gas zone, the presence of air contributes to the oxidising condition in the zone. The cryolite

content in the bath zone provides a very aggressive corrosive environment. In the metal zone, molten aluminium creates a highly reducing condition

Due to its high oxidation resistance and high stability toward molten bath, nickel ferrite could be suitable to be applied in the gas zone and bath zone. However, nickel ferrite may not be suitable to be applied in the aluminium zone since it is likely to react with aluminium that will lead to the degradation of the nickel ferrite and contamination to molten aluminium. Equilibrium calculations with 1 mol nickel ferrite and 10 mol liquid aluminium at 860 °C to 1200 °C show the dissolution of iron and nickel to aluminium as shown in Figure 2 [12]. At 965 °C, the composition of liquid phase is 62.1 % Al, 29.1 % Ni and 7.8 % Fe (Figure 1). This analysis indicate that exposure of nickel ferrite to aluminium is likely to result in severe degradation of that material, illustrating that it will difficult to find one material that can satisfy the range of chemical conditions inside the cell.

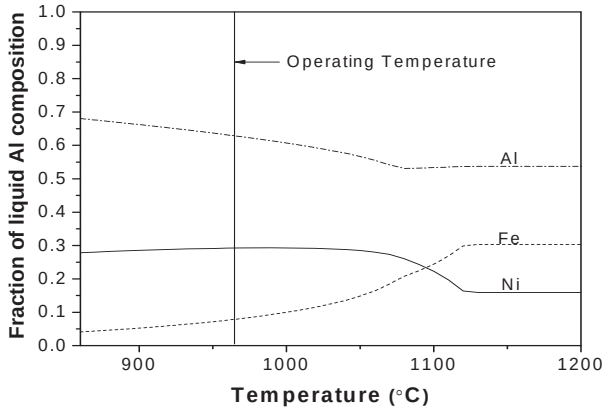

Figure 1 - Equilibrium calculations of 1 mol nickel ferrite and 10 mol aluminium showing dissolution of nickel and iron to aluminium

PROPOSED APPROACH

In this paper, author proposed multi-layer strategy and heat flux strategy to tackle the combine corrosive action of the different environments within the cell as illustrated in Figure 2. With multi-layer strategy, two or three different materials are combined. Multi-layer strategy can be applied horizontally, using three different materials in which each of the material can withstand each zone mentioned above. It can also be applied vertically, using two different materials in which one of them have high corrosion resistance while the other has low heat conductivity to maintain the heat balance of the cell.

In heat flux strategy, the amount of heat transferred through each zone of the sidewall is varied, making it possible to maintain frozen ledge in particular zone while maintaining the cell heat balance. As for example is to control heat flux through sidewall bath zone to allow ledge formation on this zone and incorporate air gaps or inserting low heat conductivity material into sidewall at the air and molten aluminium zone to minimize heat flux through this area. This strategy would reduce the material properties constrain since the sidewall does not have to withstand all the zones within the cell.

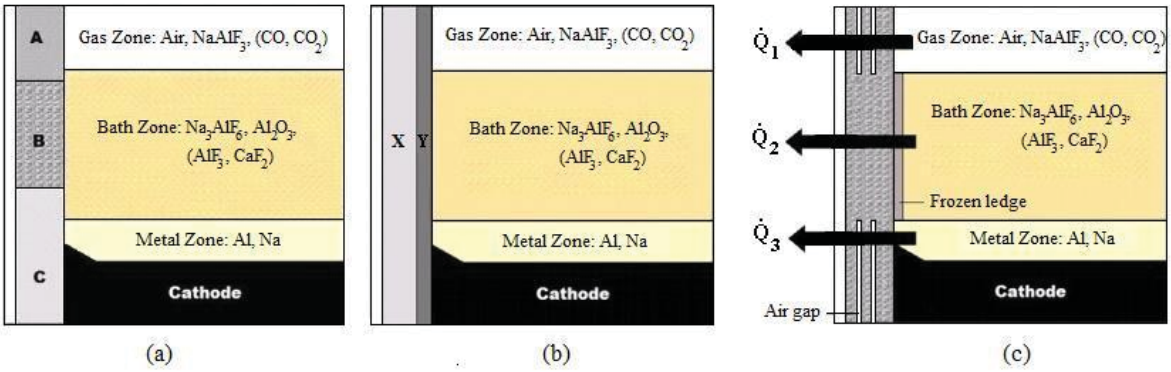

Figure 2 (a) vertical layer strategy, (b) horizontal layer strategy, (c) heat flux strategy

At this stage, these proposals are highly speculative and the authors acknowledge that there are very significant materials science, process control, maintenance and cost issues associated these ideas that are yet to be explored. It is the intention of this paper to raise awareness of these issues and stimulate further study on these exciting and challenging problems.

REFERENCES

1. H.G. Schwarz, *Technology diffusion in metal industries: driving forces and barriers in the German aluminium smelting sector.* Journal of Cleaner Production, 2008. **16**(S1): p. 37-49.
2. K. Grjotheim and B.J. Welch, *Aluminium Smelter Technology*. 2nd ed. 1988, Düsseldorf: Aluminium-Verlag.
3. J. Thonstad et al., *Aluminium Electrolysis*. 3rd ed. Fundamentals of the Hall-Heroult Process. 2001, Düsseldorf: Aluminium-Verlag.
4. M. Sørlie, and H.A. Øye, *Evaluation of cathode material properties relevant to the life of Hall-Heroult cells.* Journal of Applied Electrochemistry, 1989. **19**(4): p. 580-588.
5. G. Brooks et al., *Challenges in light metals production.* Mineral Processing & Extractive Metallurgy: Transactions of the Institution of Mining & Metallurgy, Section C, 2007. **116**: p. 25-33.
6. H. Kvande, and W. Haupin, *Inert anodes for Al smelters: Energy balances and environmental impact.* JOM, 2001. **53**(5): p. 29-33.
7. K. Downie, *$NiFe_2O_4$ as a sidewall materials in Hall-Heroult cells*, in *Faculty of Engineering*. 2007, University of Wollongong: New-South Wales.
8. R.P. Pawlek, *Inert anodes: Research, development, and potential.* Light Metal Age, 2002. **60**(1-2): p. 50-55.
9. X.Y. Yan, M.I. Pownceby, and G. Brooks. *Corrosion behavior of nickel ferrite-based ceramics for aluminum electrolysis cells*. (Warrendale, PA: TMS, 2007) p. 909-913.
10. E. Olsen, and J. Thonstad, *Nickel ferrite as inert anodes in aluminium electrolysis: Part II. Material performance and long-term testing.* Journal of Applied Electrochemistry, 1999. **29**(3): p. 301-311.
11. E. Skybakmoen, H. Gudbrandsen, and L.I. Stoen. *Chemical resistance of sidelining materials based on SiC and carbon in cryolitic melts - a laboratory study*. (Warrendale, PA: TMS, 1999) p. 215-222.
12. C.W. Bale et al., *FactSage thermochemical software and databases*, CALPHAD, 2002, **26**: p.189-228.

OXIDISED NI-BASED ANODES FOR ALUMINIUM ELECTROLYSIS: THE PROTECTIVE ROLE OF THE OXIDE SCALE

Vivien Singleton[1], Barry J. Welch[2], Maria Skyllas-Kazacos[1]

[1]Centre for Electrochemical and Mineral Processing (CEMP), School of Chemical Sciences and Engineering, University of New South Wales
[2]Welbank Consulting Ltd.

Key Words: Inert anodes, aluminium electrolysis, oxygen evolution, nickel alloys

The development of an inert oxygen-evolving anode for the Hall-Héroult process is one of the key challenges for the primary aluminium industry. Realisation of a viable inert anode could lead to significantly reduced greenhouse emissions, and the elimination of costs and process inefficiencies associated with anode changing. If combined with novel cell designs and advanced control systems, inert anodes may also be capable of reducing the overall energy requirement for aluminium production. Several research bodies claim to have conquered the fundamental materials challenges [1-3], however, a number of key questions remain about the science governing the anode behavior.

Nickel-based alloys have shown significant promise as inert anode candidates, owing to the low solubility of nickel-containing oxides in the cryolite electrolyte [4]. Effective performance can only be achieved with the formation of a protective oxide scale on the anode prior to electrolysis. The present study aims to identify the optimal scale properties for a selection of Ni-based anode candidates. The effectiveness of the scales in minimising anode wear was assessed over periods of short-term electrolysis. It was found that the anode lifetime is greatly affected by the level of scale adhesion, porosity and solubility. Scale properties must be optimised by altering the alloy composition, oxidation conditions and surface pre-treatment regime.

References

[1] S.P. Ray and R.A. Rapp, European Patent, EP122160 (1986)
[2] T.T. Nguyen and V. deNora, United States Patent, 2005/0205431 (2005)
[3] T. Nguyen and V. deNora, De Nora oxygen evolving inert metallic anode, *Light Metals 2006,* T.J. Galloway Editor, TMS, Warrendale, PA, 2006, 385-390
[4] T.E. Jentoftsen, O.-A. Lorentsen, E.W. Dewing, G.M. Haarberg, and J. Thonstad, Solubility of some transition metal oxides in cryolite-alumina melts: Part I. Soulbility of FeO, $FeAl_2O_4$, NiO and $NiAl_2O_4$, *Metall. Mater. Trans. B*, **33B**, 901-908, 2002.

A NEW ROUTE FOR PRODUCING METAL BORIDES AND CARBIDES

X.Y. Yan, M.I. Pownceby, M.A. Cooksey, and M.R. Lanyon

CSIRO Process Science and Engineering, Clayton, Victoria 3168, Australia

Keywords: Molten Salt, Electro-Reduction, Oxide, Boride, Carbide

Metal borides and carbides are non-oxide ceramics. They exhibit many attractive properties, such as wear resistance (e.g., WC, TiB_2 and TiC), oxidation resistance (e.g., SiC) and resistance to attack by molten metals or glasses (e.g., TiB_2 and TiC). Conventional processes for producing metal borides and carbides mainly include: (i) carbothermic reduction, (ii) combustion method and (iii) gas or liquid phase synthesis, among which process (i) is the primary route especially on a large-scale production [1-2]. For instance, TiB_2 and TiC are commercially produced by the carbothermic reduction of TiO_2/B_2O_3 and TiO_2/C in electric furnaces at ~2000 ºC [1, 2]. Final products are "clinkers" of fine crystals that are subsequently crushed and ground to obtain TiB_2 and TiC powders. However, it is difficult to ensure high purity of the final products due to high operating temperatures [1]. The high temperatures also cause engineering difficulties with reactor designs and materials. It is hence desirable to develop low temperature, energy efficient and low cost routes for the production of metal borides and carbides to lower energy consumptions and cut production costs. This work studies a new route for synthesizing metal borides and carbides from oxides at 600-900 ºC. The concept of the process is based on electro-reduction of oxides in $CaCl_2$-based electrolytes [3]. Sintered pellets of mixed metal oxides or metal oxide/carbon are used as the cathode while a graphite rod is employed as the anode, with both being immersed in a bath of the molten electrolyte in an electrolytic cell. On application of potentials to the cathode, less negative than cathodic deposition potentials of electrolyte cations and more negative than ionisation potentials of the oxides, the preferred cathodic reaction is the ionisation of the oxygen from the oxides termed electro-reduction of the oxides:

$$O \text{ (in oxides)} + 2e = O^{2-} \text{ (in electrolyte melt)}$$

instead of the cathodic deposition of Na and Ca in the case of molten $CaCl_2$–NaCl eutectic. The anodic reactions with a carbon or O_2-evolving inert anode is given respectively by

$$O^{2-} - 2e + 1/xC = 1/xCO_x\,(g);\ \ (x = 1 \text{ or } 2)$$

$$O^{2-} - 2e = 1/2O_2\,(g)$$

The Cl^- in the electrolyte is unlikely to be discharged at the anode. In this work, two examples for production of TiB_2 and TiC are provided to demonstrate the technical viability of this molten salt route.

Table I lists cathodic ionisation reactions of various oxides and their standard electrode potentials (E°) vs. $E^\circ_{Ca^{2+}/Ca} = 0$ V, calculated from thermodynamic data [4]. As can be seen, the oxides can be reduced by cathodic oxygen ionisation without decomposing NaCl or $CaCl_2$. Furthermore, a direct formation of TiB_2 or metal carbides from a mixture of TiO_2/B_2O_3 or metal oxide/C can occur at less cathodic potentials than those of electro-reduction of individual metal oxides to metals or B_2O_3 to B, thus promoting the electro-reduction of the oxides, which can in turn lower theoretical minimum energy requirements for this electrolytic reduction route.

Table I. Possible cathodic reactions and their standard electrode potentials (E°) [4]

Cathodic reaction	E° vs. ($E^\circ_{Ca^{2+}/Ca} = 0$ V)	
	600 °C	900 °C
$1/3WO_3 + 1/3C + 2e = 1/3WC + O^{2-}$	1.81	1.77
$1/3WO_3 + 2e = 1/3W + O^{2-}$	1.75	1.71
$1/2TiO_2 + 1/2C + 2e = 1/2TiC + O^{2-}$	1.24	1.20
$1/5TiO_2 + 1/5B_2O_3 + 2e = TiB_2 + O^{2-}$	1.19	1.14
$1/2SiO_2 + 1/2C + 2e = 1/2SiC + O^{2-}$	1.03	1.00
$1/3CaTiO_3 + 1/3C + 2e = 1/3TiC + 1/3Ca^{2+} + O^{2-}$	1.01	0.97
$1/3B_2O_3 + 2e = 2/3B + O^{2-}$	1.01	0.95
$1/2ZrO_2 + 1/2C + 2e = 1/2ZrC + O^{2-}$	0.89	0.86
$1/2SiO_2 + 2e = 1/2Si + O^{2-}$	0.87	0.84
$1/2TiO_2 + 2e = 1/2Ti + O^{2-}$	0.78	0.76
$1/5Ca_2B_2O_5 + 2e = 2/5B + 2/5Ca^{2+} + O^{2-}$	0.66	0.62
$1/3CaTiO_3 + 2e = 1/3Ti + 1/3Ca^{2+} + O^{2-}$	0.56	0.53
$1/2ZrO_2 + 2e = 1/2Zr + O^{2-}$	0.40	0.38
$Na^+ + e = Na$	0.02	0.06
$Ca^{2+} + 2e = Ca$	0.00	0.00

Figure 1 shows the I-t curves for the sintered pellets of TiO_2/B_2O_3 (curve A) and TiO_2/C (curve B) during electrolysis up to 15 h, where currents jumped when imposing 3.1 V to the cell followed by current decays at different rates due to different rates of the oxygen removal from the cathode materials. The currents declined steadily after about 4 h of electrolysis until the termination of electrolysis. These suggested decreasing oxygen contents of the cathode materials. Curve B had less initial current peaks and values than those of curve A over 0-4 h, indicating that more oxygen was removed from the TiO_2/B_2O_3 pellets than the TiO_2/C ones. An analysis by XRD of the cathode products revealed that the reduced TiO_2/B_2O_3 pellets contained TiB_2 (major) and TiB (minor), free of oxides, whilst TiC was the major phase and $CaTiO_3$ and C were the minor phases in the TiO_2/C pellets. Figures 2a and b show the SEM images of the TiB_2 and TiC particles produced, with the EDS spectra on each image shown in Figs. 2c and d. The sub-micron TiB_2 grains were clustered together as larger agglomerates of 20-30 μm in size. The plate-like TiC particles were stacked together as a larger particle. There were sub-micron grains within each TiC plate. The EDS results showed that the electro-reduced TiO_2/B_2O_3 or TiO_2/C sample mainly consisted of Ti and B (in Fig. 2c) or Ti and C (in Fig. 2d), where a minor amount of Ca, Na, or Cl resulted from the residual electrolyte. The above results demonstrated that metal borides and carbides, such as TiB_2 and TiC, were produced from their oxide precursors using the present molten salt route. A detailed understanding of the electrochemistry and possible reduction mechanisms involved in the process has been described elsewhere [5]. Compared to the existing routes [1, 2], the present molten salt route has the advantages

of higher product purities due to easier controls of reactant ratios, much lower operating temperatures and possible use of O_2-evolving inert anodes to make the new route a "green" process.

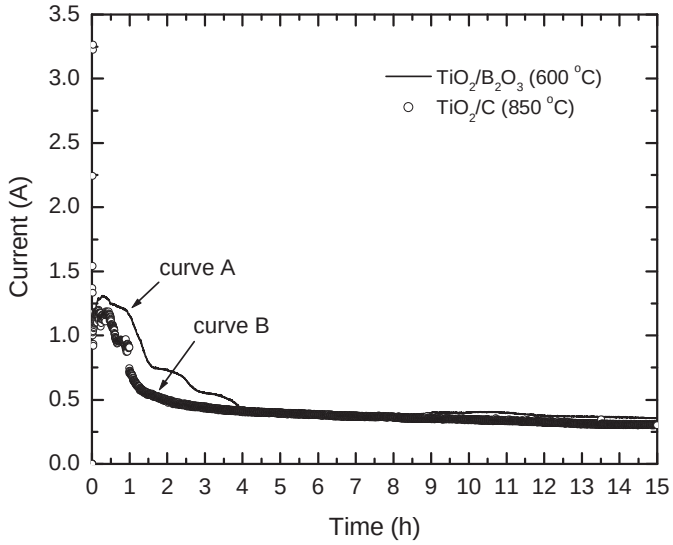

Figure 1 - Current-time curves of the sintered pellets at 3.1 V

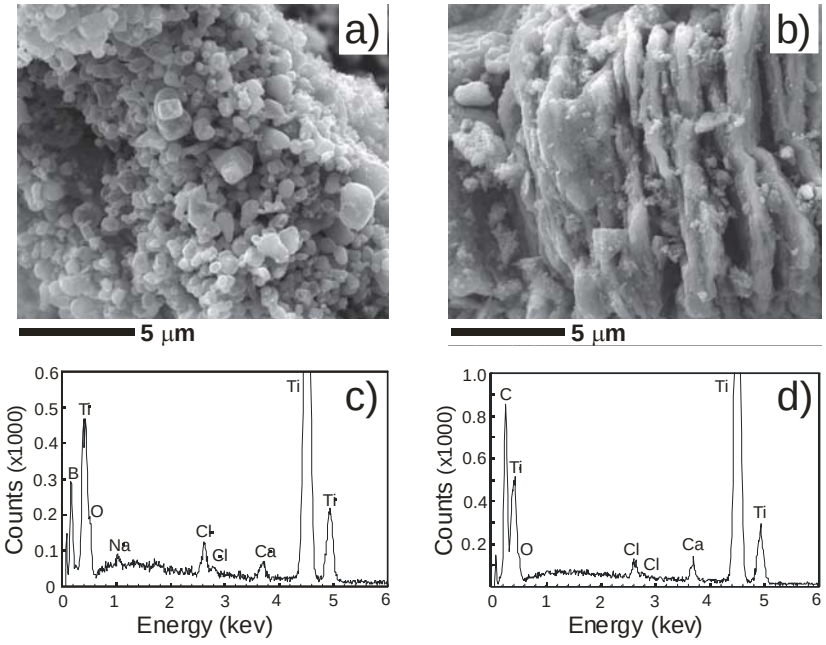

Figure. 2 - (a), (b) SEM images of the reduced TiO_2/B_2O_3, TiO_2/C pellets; (c), (d) EDS spectra on the images (a), (b)

In summary, a new molten salt route was investigated for the production of metal borides and carbides directly from metal oxides, boric oxide, and carbon powders by electro-reduction. The thermodynamic analysis showed that the oxides can be electro-reduced without decomposing NaCl and $CaCl_2$ and the direct formation of TiB_2 or metal

carbides from TiO_2/B_2O_3 or metal oxide/C mixtures by oxygen ionisation at the cathode is more favorable compared to those of individual pure oxides. Micro-sized powders of TiB_2 and TiC were readily prepared directly from the oxide and graphite powder precursors by electro-reduction in molten $CaCl_2$-NaCl eutectic at 600-900 ºC, through which it was demonstrated that metal borides and carbides can be produced using this new route.

References

[1] A. W. Weimer, *Carbides, Nitride and Boride Materials Synthesis and Processing*, Chapman & Hall, London, 1-38, 75-753, 1997.

[2] P. Schwarzkopf and R. Kieffer, *Refractory Hard Metals: Borides, Carbides, Nitrides, and Silicides*, The Macmillan Company, New York, 1953.

[3] D.J. Fray and R.C. Copcutt, Intermetallic Compounds, *WO 02/40748 A1*, 23 May, 2002.

[4] *HSC Chemistry for Windows*, Version 5.1, Outokumpu Research Oy, 2002.

[5] X.Y. Yan, M.I. Pownceby, M.A. Cooksey, and M.R. Lanyon, Preparation of TiC Powder and Coatings by Electro-deoxidation of Solid TiO_2 in Molten Salts, *Trans. Inst. Min Metall. C*, **118**, 23-34, 2009.

CONSTRUCTION AND APPLICATION OF PHASE DIAGRAMS FOR HIGH TEMPERATURE PROCESSING

Hector M. Henao
PYROSEARCH Centre
The University of Queensland

New experimental procedures have been developed by the Pyrometallurgy Research Centre (PYROSEARCH) at the University of Queensland that have resolved a number of experimental difficulties associated with phase equilibria determination in slag systems. The experimental procedures involve high temperature equilibration and quenching followed by electron probe X-ray microanalysis. This technique has been used to construct the phase equilibrium diagrams in the multi-component systems relevant to the pyrometallurgy production of Fe, Pb, Zn, Cu, recycling of metals and coal slags. This presentation discusses the advantages, last developments, improvements and applications of the technique for high temperature processing.

VISUALIZATION OF ALUMINIUM INITIAL STAGE OXIDATION

Behrooz Fateh[a,1,3], Geoff Brooks[a,1], M. Akbar Rhamdhani[a,1], John A. Taylor[a,2], Jeff Davis[3] and Martin Lowe[3]

[a] CAST Cooperative Research Centre (CAST CRC)
[1] High Temp Group, Faculty of Engineering and Industrial Science, Swinburne University of Technology
[2] School of Mechanical & Mining Engineering, University of Queensland
[3] The Centre for Atom Optics and Ultrafast Spectroscopy (CAOUS), Swinburne University of Technology

Keywords: Femto-second laser ablation, fast imaging, Al initial oxidation

Aluminium is among the metals with the greatest affinity for oxygen. Aluminium oxidation is a process that occurs easily and rapidly. At room temperature Al is always covered with an oxide film (2-3 nm in thickness) [1]. The study of initial oxidation is very important as it concerns the first step of a metal's oxidation and corrosion behaviour. The characteristics of the kinetics of early-stage oxidation are believed to have an important influence on the later steady-state growth. Furthermore, there are many aspects of Al melt handling and cast process that results in oxidation of Al and dross formation. Dross is an inhomogeneous complex mixture of aluminium oxides along with entrapped molten metal. Dross formation in melt handing process leads to a huge profit loss [2].

In order to quantify the Al oxidation kinetics, the process of oxide layer formation upon solid aluminium following ablation of the surface with an ultra-fast laser beam and using fast imaging were studied. For the ablation of solid Al surface, the laser experimental set up was optimized. The sample was placed in a vacuum chamber with a silica viewer (50 mm diameter) for optical access. The chamber was connected to a rotary pump producing a vacuum of 2 mTorr. The vacuum chamber was clamped to a two-dimensional positioning system which was interfaced to a Labview control system. Laser and imaging light sources were focused through two different optical lenses. The reflected light was then imaged to a high speed camera. A high speed camera and the laser beam were synchronized by means of introducing the trigger pulse to a fast shutter. The laser beams were focused and hit the Al surface in angle of 45 degree. In order to make shallow holes, number of shots and laser intensity were optimised. The live images of ablated Al surface and the formation of sparks during laser ablation showed that 40 shots with 7-8 mWs power are enough to remove the oxide layer on the Al specimen. In order to capture images by high speed camera, a very strong light source is necessary. Thus, illumination of Al surface was a challenging issue. Focusing a very bright light source using lenses and a fibre optic light were optimized. The camera adjusted to take 3000 frames per second in full resolution. Finally, the time evolution of the oxide layer on the ablated surface was recorded.

Figure 1 shows the schematic of the laser ablation and imaging techniques and Figure 2 shows the photos of the experimental set-up, consisting vacuum chamber, objective

lenses, mirrors, camera, filters, beam splitter, none- linear BBO crystal and the laser beam.

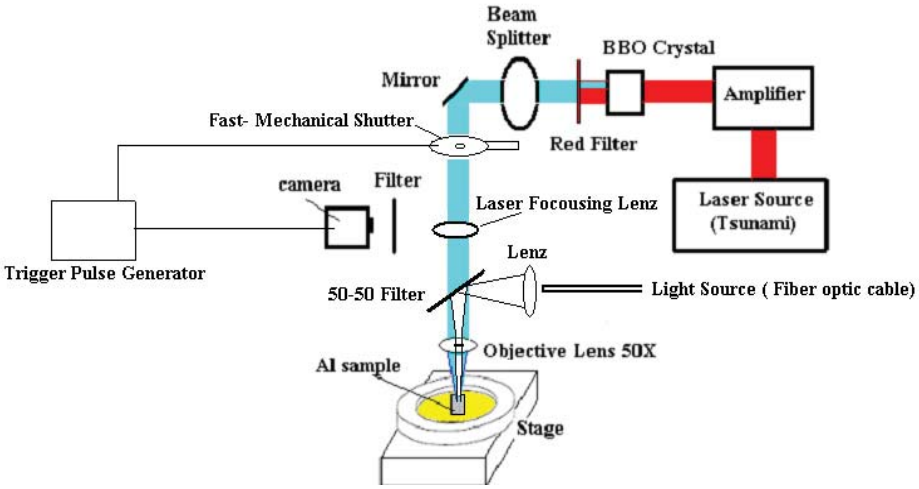

Fig. 1 Laser ablation experimental set-up

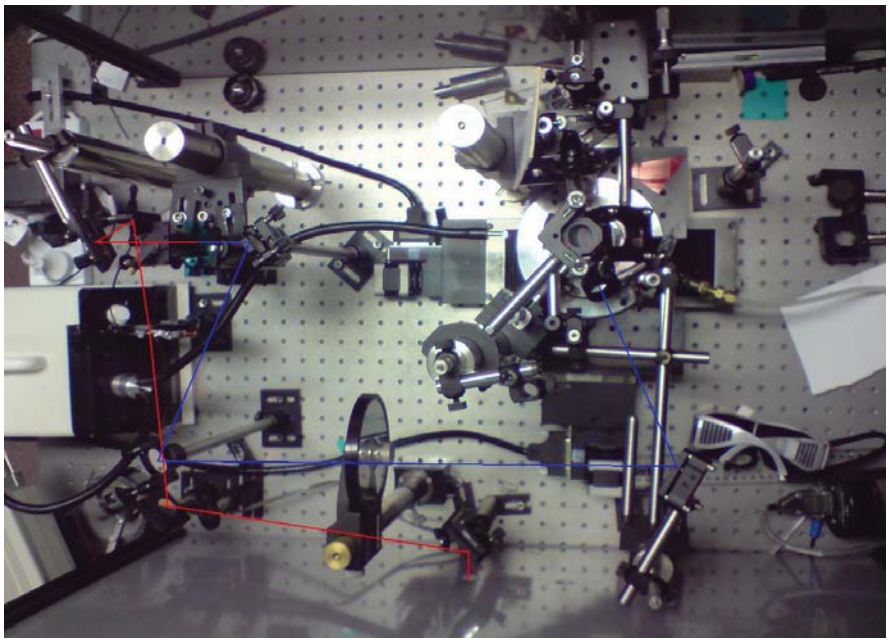

Fig. 2 The photo of the experimental set-up

References

[1] K. Shimizu, K. Kobayashi, G.E. Thompson G and G.C. Wood, *Oxid. Met.*, 36 (1991), p.1
[2] J. Taylor and A. Deev; "The *Oxidation of Molten Aluminium and its Alloys*"; CAST Report; 2006

KINETICS OF SILICOTHERMIC REDUCTION OF CALCINED DOLOMITE IN FLOWING ARGON ATMOSPHERE

Winny Wulandari[1], Geoff Brooks[1], M. Akbar Rhamdhani[1], and Brian J. Monaghan[2]
[1]Swinburne University of Technology
[2]University of Wollongong

Keywords: silicothermic, kinetics, magnesium

The Pidgeon process is currently the dominant silicothermic process route to produce magnesium. Calcined dolomite is briquetted with ferrosilicon and reduction is carried out at 1100 – 1200 ^{o}C. The reduction can be written as:

$$2\ CaO.MgO_{(s)} + xFeSi_{(s)} \rightarrow 2Mg_{(g)} + Ca_2SiO_{4(s)} + xFe_{(s)} \quad (1)$$

The magnesium vapour extracted is removed using vacuum condition to condense as a dense metal. Thermodynamic analysis of this process has been carried out in the past to predict the distribution of the metal impurities in condensed magnesium. The results suggested that a number of impurities in different phases formed in the region between reaction zone and condenser. The thermodynamic results only are not sufficient to describe the process, and the knowledge of the kinetics of the Pidgeon process is required. Kinetics plays important role to give more insight to the process such as for process design and control.

The kinetics phenomena in the Pidgeon process are relatively complex. It is a heterogeneous reaction which includes three different solid react and produce vapour and another solids. There have been a number of kinetic studies of the Pidgeon process in vacuum condition, but very limited literature available for the reduction in flowing inert gas atmosphere. The kinetics phenomena will include the intrinsic chemical kinetics of reaction, transfer of magnesium vapour to the surface through pores, and transfer of vapour from the surface to the bulk.

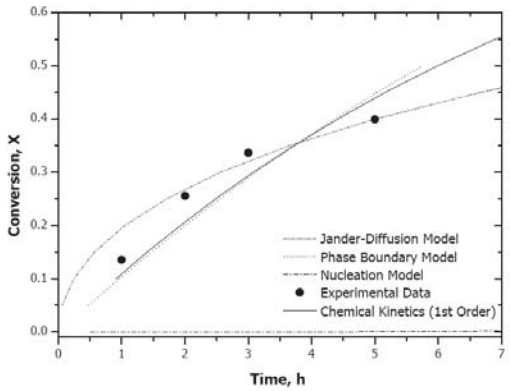

Figure 1. Comparison of Different Kinetic Models and Experimental Data of Magnesium Recovery at 1150 ^{o}C.

In this study, the experimental data from Morsi *et al* [1] which studied silicothermic in flowing argon at 0.08 L/min to 1 L/min was analysed using a number of kinetic models

based on the controlling step, such as diffusion models, phase boundary model, nucleation model, and intrinsic chemical reaction model. Diffusion model can represent the experimental data as described in Figure 1. The available diffusion models were also examined. The three dimension diffusion models, such as Jander, Serin-Ellickson, Ginstling-Brounshtein, and Valensi-Carter models can represent the experimental data, as seen in Figure 2, with the Ginstling-Brounshtein model $(1-2/3X(1-X)^{2/3} = Kt)$ and Jander model $([1-(1-X)^{1/3}]^2 = Kt)$ fit mostly the experimental data at different operating temperature. This suggests that the overall reaction is controlled by diffusion of solid reactant through the product layer.

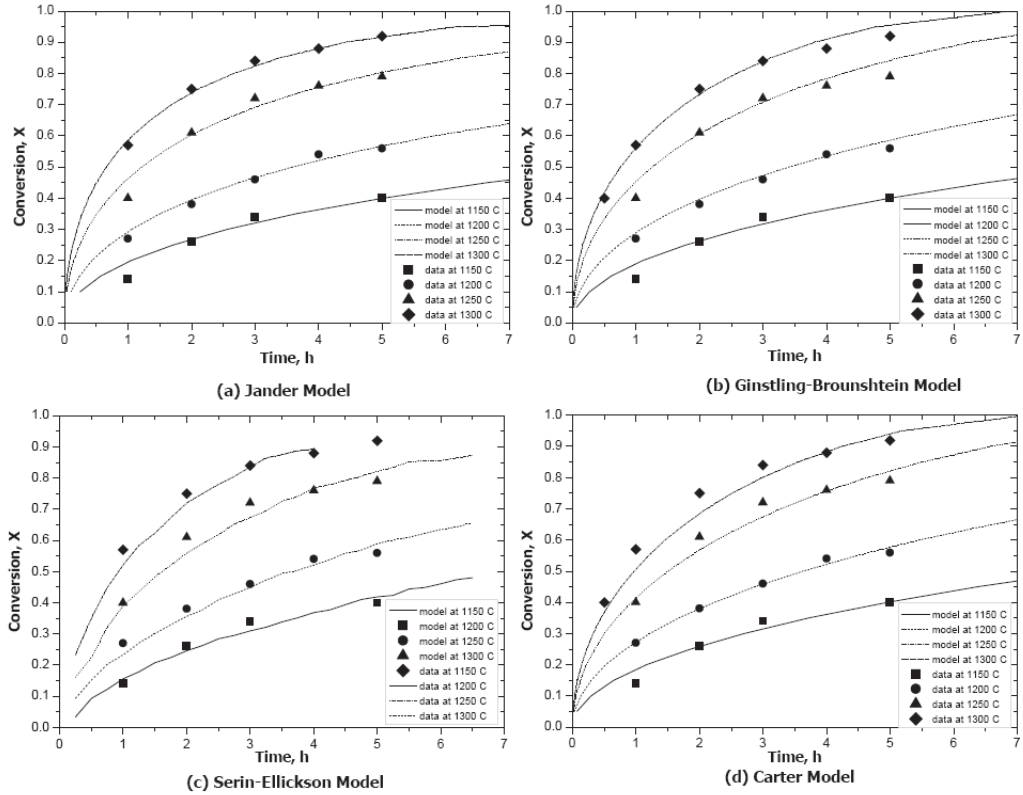

Figure 2. Three Dimensional Diffusion Models

Mass transfer effect of magnesium vapour from the surface to the bulk was also observed. The calculations were also based on Morsi et al's data. On the mass transfer of magnesium vapour, the transfer of magnesium vapour through the pores is found via Knudsen diffusion.

The mass transfer is expressed as:

$$j = \frac{M}{RT} K_c (P_B - P_S) \qquad (2)$$

where j is magnesium diffusion flux ($gcm^{-2}s^{-1}$), K_c is mass transfer coefficient, P_B is the pressure of magnesium in the bulk, and P_S is pressure of magnesium at the surface of briquette. The mass transfer coefficient is calculated by Warner relation [2], which is a modified Ranz-Marshall relation [3] for the gas stream passed in the tube:

$$K_c = \frac{1.15D}{2r_s}\left(2.0 + 0.6N_{\mathrm{Re}}^{1/2}N_{Sh}^{1/3}\right) \quad (3)$$

r_s is radius of the pellet, N_{Re} is Reynold number, and N_{Sc} is Schmidt number. The magnesium diffusivity and viscosity is calculated from Chapman-Enskog theory. The results are presented in Figure 3. The external mass transfer of magnesium vapour to the bulk phase is quite small. With Kc is 9 to 10 cm.s^{-1}, which resulted to pressure drop of 1 to 2 mmHg. These results suggest that at low flow rate, argon gas is saturated with magnesium vapour.

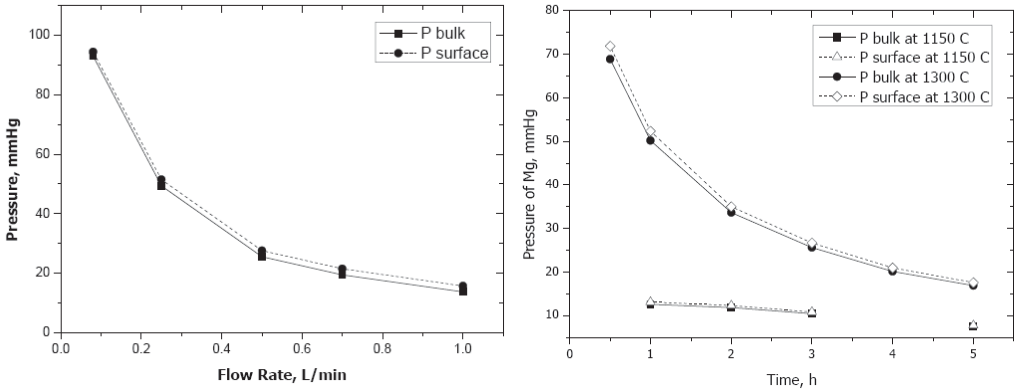

Figure 3. Calculated Pressure of Magnesium Vapour in the Surface of Briquette and Bulk Phase with (a) Different Flow Rate, and (b) Different Reaction Time

Reference:

1. Morsi, I.M., et al., Silicothermic Reduction of Dolomite Ore Under Inert Atmosphere. Canadian Metallurgical Quarterly, 2002. **41**(1): p. 15-28.
2. Warner, N.A., Trans. TMS - AIME, 1964. **230**: p. 163-176.
3. Ranz, W.E. and W.R. Marshall. Jr, Chemical Engineering Progress, 1952. **48**: p. 141-146, 173-180.

AUTOMATED ALUMINIUM SIPHONING SYSTEM

Guangwei Liu
Major Furnace Australia Pty Ltd, 100 Fairbank Rd, Clayton, Victoria, 3169, Australia

Keywords: Aluminium Siphoning, Automated Siphoning, Rio Tinto Alcan – Major Siphon system

Siphoning has long been recognised as a method of transferring molten aluminium from reduction crucibles to Casthouse holding furnaces which generates the least amount of dross. This paper will present and discuss the Rio Tinto Alcan – Major automated siphon system that is finding application in installations in large Aluminium smelters.

Background to Automated Siphoning

Siphoning has been used to transfer aluminium from crucibles to furnaces for more than 40 years. A manual system was originally devised by Alcan, which performed adequately in the hands of skilled operators but lacked operational refinement and user friendliness needed to encourage a wider acceptance.

As part of its dross reduction programme, Comalco Aluminium carried out siphoning trials at its NZAS smelter in 1992. Following very positive results, in 1994, Comalco (now Rio Tinto Alcan) developed an automated siphon system for use on the continuous atomising process at its powder plant at Bell Bay, Tasmania. The success of this system encouraged the installation of a system which married the Comalco developed siphon automation to a specially engineered pipe handling system designed by Major for the third potline expansion at the Boyne Smelter, Queensland. This system was commissioned in 1997 and involved the conversion of 12 existing holding furnaces from cascade pouring to siphoning. The Boyne smelter currently siphons 550,000 tonnes of aluminium annually through 14 furnaces.

In 2008 the 'green field' smelter at Sohar in Oman was commissioned with four automated siphon systems designed by Major.

The Rio Tinto Alcan - Major Siphon System

After 11 years of operation and ongoing refinement, the Rio Tinto Alcan – Major (RTA- Major) automated siphoning system has demonstrated proven reliability and robustness. The automated siphoning process is regarded as inherently safer than other transfer methods, mainly due to the ability to instantly stop the metal flow by releasing the vacuum in the event of a problem.

As the process is intentionally 'quiescent' in normal operation, siphoning provides very little natural feedback to the operator, so the automation includes a control interface and closed circuit TV system designed to inform the operator of the system status and identify problems if they occur.

The key functional parts of the system are: the siphon pipe handling & pre-heating system; the siphon vacuum control system; the operator interface; pipe transport and maintenance equipment and the furnace interlocks.

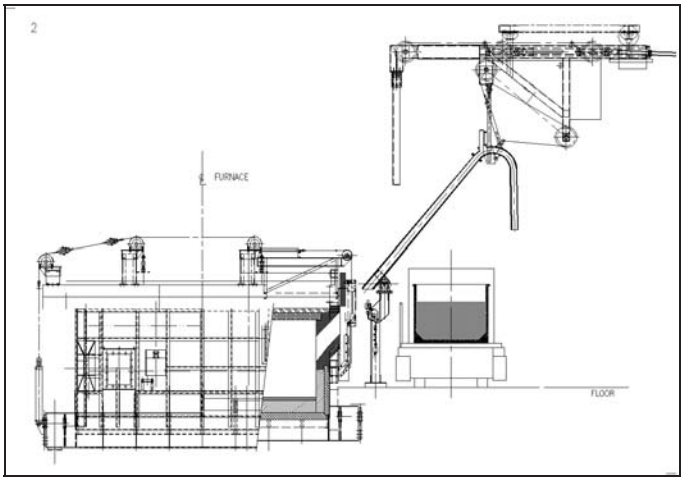

Smelter siphoning arrangement showing the RTA - Major pipe handling system

The RTA- Major siphon pipe handling system has been designed to suit a typical smelter cast house arrangement with holding furnaces aligned adjacent to a hot metal delivery passage. Siphon pipes are parked overhead in the hot metal passage, in line with each furnace (Figure 1). While the siphons are parked on standby, gas fired pre-heat burners maintain the pipes at temperature to eliminate moisture, reduce metal chill and minimise thermal shock to the cast iron siphon pipes.

When a crucible of metal arrives on a hot metal carrier vehicle, the siphon pipe is lowered to simultaneously enter the crucible and the holding furnace, by a simple pushbutton operation. The crucible is tilted to about 5^{o} to concentrate the metal under the pipe inlet and so minimise the residual metal heel. Once the siphon pipe is in position, the siphon vacuum sequence is started, which automatically empties the crucible at a controlled rate. When the crucible becomes empty, the vacuum is automatically released and the siphon pipe is returned home to its parked position.

The operator is provided with a closed circuit TV to monitor the metal level in the crucible. This visual feedback, along with real time display of process variables and alarm messages ensures the operator is kept constantly informed of the process status from a safe location at the operator control station. The RTA - Major system also facilitates safe and efficient removal, replacement and transport of siphon pipes to and from the pipe cleaning bay. Regular cleaning and maintenance of siphon pipes is essential for reliable siphon system operation.

The basic steps involved in siphoning a crucible of metal are: Position the crucible vehicle; Tilt the crucible; Lower the siphon pipe into the furnace; Initiate the vacuum cycle; Return the siphon to its parked position. This sequence can normally be completed in 8 to 10 minutes for a 10 tonne crucible.